University of California
Center for Economic
Competitiveness in
Transportation

UCONNECT

Sustainable Operation of Arterial Networks

Final Report

Pravin Varaiya, UC Berkeley

Sponsored by

Caltrans

2017

Berkeley UC Irvine UCLA UCR UCSB CAL POLY POMONA

STATE OF CALIFORNIA • DEPARTMENT OF TRANSPORTATION

TECHNICAL REPORT DOCUMENTATION PAGE

TR0003 (REV 10/98)

ADA Notice

For individuals with sensory disabilities, this document is available in alternate formats. For information call (916) 654-6410 or TDD (916) 654-3880 or write Records and Forms Management, 1120 N Street, MS-89, Sacramento, CA 95814.

1. REPORT NUMBER	2. GOVERNMENT ASSOCIATION NUMBER	3. RECIPIENT'S CATALOG NUMBER
CA17-3001		

4. TITLE AND SUBTITLE	5. REPORT DATE
Sustainable Operation of Arterial Networks	07/09/2017
	6. PERFORMING ORGANIZATION CODE

7. AUTHOR	8. PERFORMING ORGANIZATION REPORT NO.
Dileep Kalathil, Alex A. Kurzhanskiy, Pravin Varaiya	N/A

9. PERFORMING ORGANIZATION NAME AND ADDRESS	10. WORK UNIT NUMBER
University of California at Berkeley Institute of Transportation Studies 109 McLaughlin Hall Berkeley, CA 94720	11. CONTRACT OR GRANT NUMBER 65A0529 TO 041

12. SPONSORING AGENCY AND ADDRESS	13. TYPE OF REPORT AND PERIOD COVERED
California Department of Transportation Division of Research Innovation & Systems Information P.O. Box 942873 Sacramento, CA 94273-0001	Final Report, 3/1/15 – 2/29/16 14. SPONSORING AGENCY CODE

15. SUPPLEMENTARY NOTES

16. ABSTRACT

This report describes operational data analysis and modeling of arterial networks with signalized intersections as follows: The setup for data collection, analysis and simulation is presented in Section 2.1. Detailed analysis of collected signal phasing and traffic data is provided in section 2.2. Arterial traffic and platoon modeling is described in Section 2.3. Simulation results of the Rollins Park network is discussed in Section 2.4.

Research conducted under this task is an important stepping stone for building a three-level information and control system for urban networks with high-density traffic. In this task researchers focused on elements of link-level information (signal phasing and timing (SPaT) estimation and prediction) and vehicle-level control (Adaptive Cruise Control (ACC) and Cooperative Adaptive Cruise Control (CACC)). In SPaT analysis researchers presented several novel algorithms to estimate the residual duration of a signal phase for a semi-actuated intersection. These algorithms predict the times for all future phase transitions, based on previous phase measurements and on the real time information that locates the current time within the current phase. With respect to the vehicle-level control, researchers analyzed sensitivity of intersection throughput to car following models and related parameters. The Improved Intelligent Driver Model (IIDM) was chosen for traffic simulation. Finally, researchers implemented the platoon model in Simulation of Urban MObility (SUMO) and tested it in simulation of scenarios on Rollins Park network.

17. KEY WORDS	18. DISTRIBUTION STATEMENT
SPaT, Data Analysis, Protschky, Prediction, Loss Functions, Traffic Modeling, Car Following Model, Micro, Macro, ACC, CACC, Platoon Model, Simulation, Rollins Park Network	No restrictions. This document is available to the public through the National Technical Information Service, Springfield, VA 22161

19. SECURITY CLASSIFICATION *(of this report)*	20. NUMBER OF PAGES	21. COST OF REPORT CHARGED
Unclassified	73	

DISCLAIMER STATEMENT

This document is disseminated in the interest of information exchange. The contents of this report reflect the views of the authors who are responsible for the facts and accuracy of the data presented herein. The contents do not necessarily reflect the official views or policies of the State of California or the Federal Highway Administration. This publication does not constitute a standard, specification or regulation. This report does not constitute an endorsement by the Department of any product described herein.

For individuals with sensory disabilities, this document is available in alternate formats. For information, call (916) 654-8899, TTY 711, or write to California Department of Transportation, Division of Research, Innovation and System Information, MS-83, P.O. Box 942873, Sacramento, CA 94273-0001.

Sustainable Operation of Arterial Networks

Dileep Kalathil, Alex A. Kurzhanskiy, Pravin Varaiya, Jose Perez

July 14, 2017

Contents

List of Figures

List of Tables

Acknowledgement

We would like to express great appreciation to our colleagues Zahra Amini, Sam Coogan, Christopher Flores, Mike Hui, Rene Sanchez, Armin Askari, Daniel Farias and Jules Pommies for their comments and ideas.

This research was sponsored by the Division of Research, Innovation and System Information (DRISI) of the California Department of Transportation.

Chapter 1

Introduction

1.1 Overview

This report describes operational data analysis and modeling of arterial networks with signalized intersections. It is organized as follows.

- Section 2.1 presents the setup for data collection, analysis and simulation.
- Section 2.2 provides detailed analysis of collected signal phasing and traffic data.
- Section 2.3 describes arterial traffic and platoon modeling.
- Section 2.4 discusses simulation results of the Rollins Park network.

1.2 Problem

A 2013 report from US Public Interest Research Group (PIRG) [47] showed that the average number of miles driven by the average American has been falling for about a decade, through economic booms and busts, and was down to mid-1990s levels. Millennials, our nation's largest-ever generational cohort, are using transit and bikes more and taking fewer and shorter car trips, resulting in a 23% drop in the average

number of miles driven. The percentage of high school seniors with a driver's license fell 12%. Walkable city life is increasingly attractive to both young people and retiring baby boomers. The rise of on-line shopping, social media, online video streaming and telecommuting has meant fewer quick car trips.

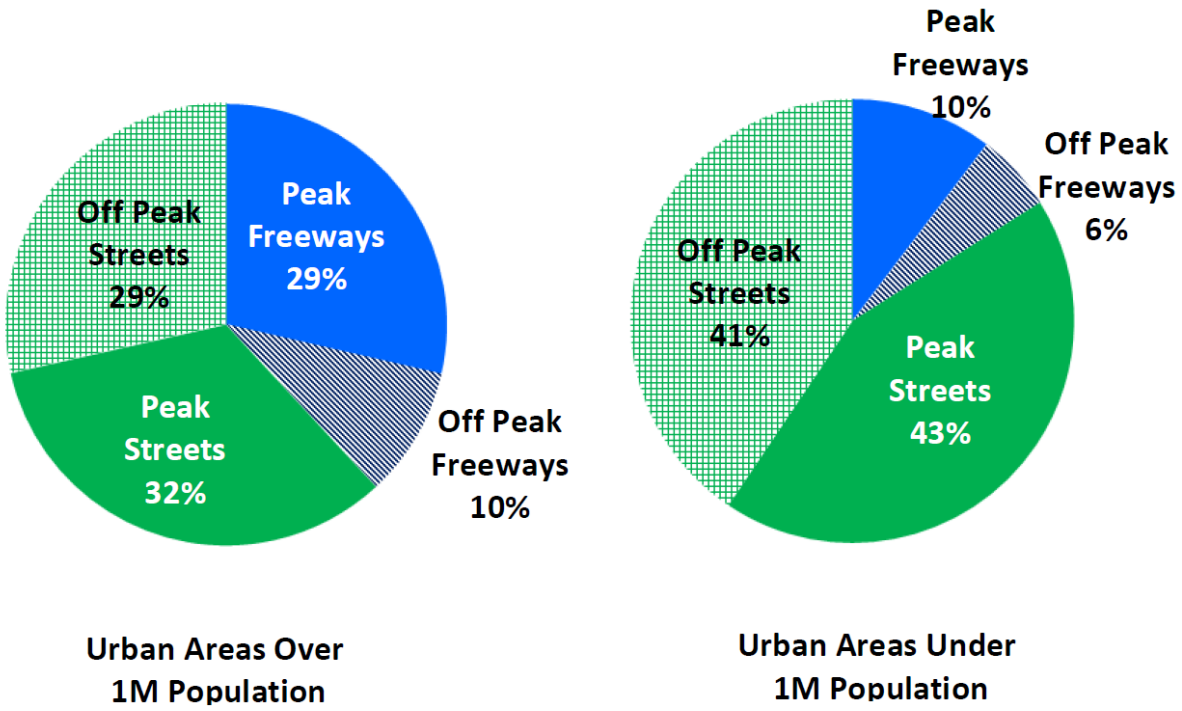

Figure 1.1: Percent delay by road type and time of day. Source: [42].

Despite these trends, as every driver knows, our roads are increasingly congested — not everywhere or all the time, but for increasing periods at a growing number of key intersections and road segments. Congestion radically reduces the volume of traffic passing through a road section, the throughput, thereby creating a negative feedback loop that creates more backups. 2015 Urban Mobility Scorecard [42] estimates that the average US commuter wastes 42 hours and 19 gallons of fuel per year because of congestion. This amounts to $960 annual congestion cost per commuter, which translates to $160B congestion cost nation-wide. As is evident from Figure 1.1, almost two thirds of congestion in large cities (and more than 80% in smaller urban areas) occur on city streets, and half of it happens during off-peak hours. The off-peak congestion affects not just private travelers, but shipping industry and manufacturers that depend on timely delivery of material. The off-peak congestion is also an evidence of poor transportation management.

The effectiveness of arterial congestion management depends on efficiency of signalized intersections. This can be explained as follows. The Highway Capacity Manual (HCM) [8] defines an intersection's capacity

as:

$$C = \sum_i s_i \frac{g_i}{T}, \tag{1.2.1}$$

where T s the signal cycle time; for lane group i, s_i is the saturation flow rate; and g_i/T is the effective green ratio. HCM takes $s_i = N \times s_0 \times f$: N is the number of lanes in the group, s_0 is the base rate in vehicles per hour (vph), and f is an 'adjustment factor' that accounts for the road geometry and nature of the traffic. The base rate s_0 is obtained from a thought experiment: it is the maximum discharge rate from an infinitely long queue of vehicles facing a permanently green signal. HCM recommends $s_0 = 1900$ vph, although empirical estimates can be as low as 1200 vph. Note that $s_i \times (g_i/T)$ is the rate at which vehicles in queue in group i can potentially be served by the intersection So we also call it the service rate in a queuing model of this lane group.

Consider an intersection with four approaches, each with one through lane and one left-turn lane as in Figure 1.2 (top). There are thus eight movements in all. Suppose each lane supports a flow up to 1900 vph for a total capacity of $1900 \times 8 = 15,200$ vph. However, from Figure 1.2 (bottom) only two movements can safely be allowed at the same time, so the effective green ratio for each movement is at most 0.25, and from equation (1.2.1) the capacity of the intersection is only 3800 vph. Thus the intersection is the principal bottleneck in urban roads: its capacity is a fraction (here 1/4) of the capacity of the roads connecting to it.

Figure 1.3 (left) is a schematic of the system of vehicle detectors installed at an intersection in Santa Clarita, CA. Each tiny white dot is a magnetic sensor that reports the times at which a vehicle enters and leaves its detection zone. When there is a pair of detectors, like at every stop bar and some advance locations, the speed of the vehicle is also estimated and reported. The detection system also receives the signal phase timing from the conflict monitor card in the controller cabinet (not shown in the figure). The sensors in the departure lanes are used to estimate turn movements, as explained in [30]. These measurements can be processed to obtain all intersection performance measures, including V/C (volume to capacity) ratios, fraction of arrivals in green, as well as red-light violations [12, 29]. From the times, at which each vehicle enters the intersection we get the empirical saturation flow rate, that is the rate at which vehicles actually move through the intersection during the green phase, and the vehicle headway.

Figure 1.3 (top right) displays the trace of all 12 vehicles that enter a through lane in the intersection during

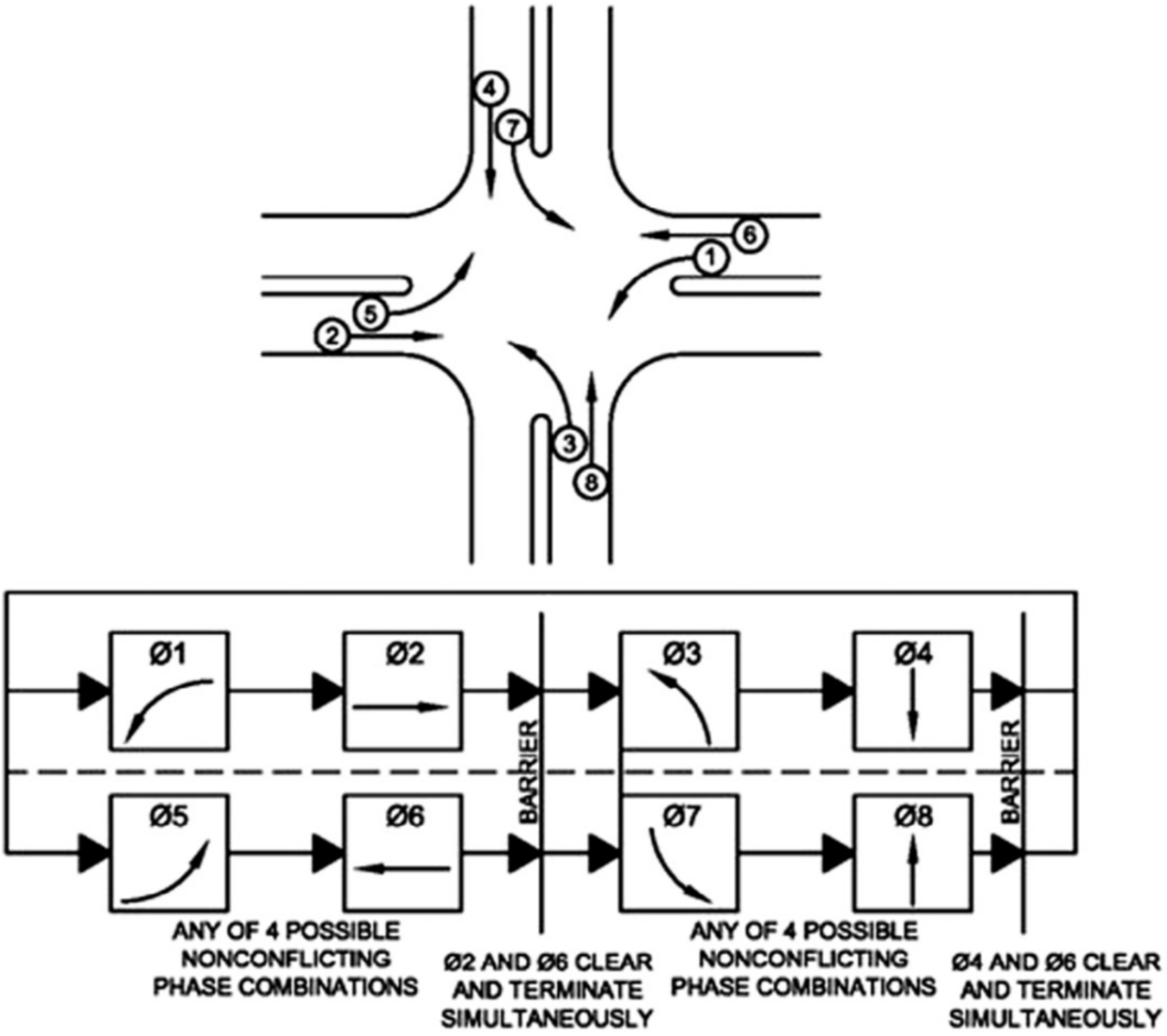

Figure 1.2: An intersection with four approaches, each with a through and left-turn movement (top), and a ring-and-barrier diagram to organize the movements (bottom). Source: [15].

one cycle with a green phase duration of 50 seconds for the through movement. The second and third columns give the times (in seconds) after the start of green and before the end of green when each vehicle enters the intersection, the fourth column gives the duration of time the vehicle 'occupied' the detector zone, and the fifth column lists an estimate of its speed. The detectors have a sampling frequency of 16 Hz, so the speeds are quantized (the distance between the two detectors is 12 feet), and speeds above 60 mph have a quantization error of about 15 mph, speeds below 30 mph have an error under 5 mph. The average speed of the 12 vehicles is 42 mph. The speed limit at this intersection is 50 mph. The first vehicle entering the intersection has a delay or reaction time of 3.47 seconds. The first 5 vehicles enter within 14.16 seconds, so the empirical saturation flow rate of this movement is 14.16/5 = 2.83 seconds per vehicle or 3600/2.83

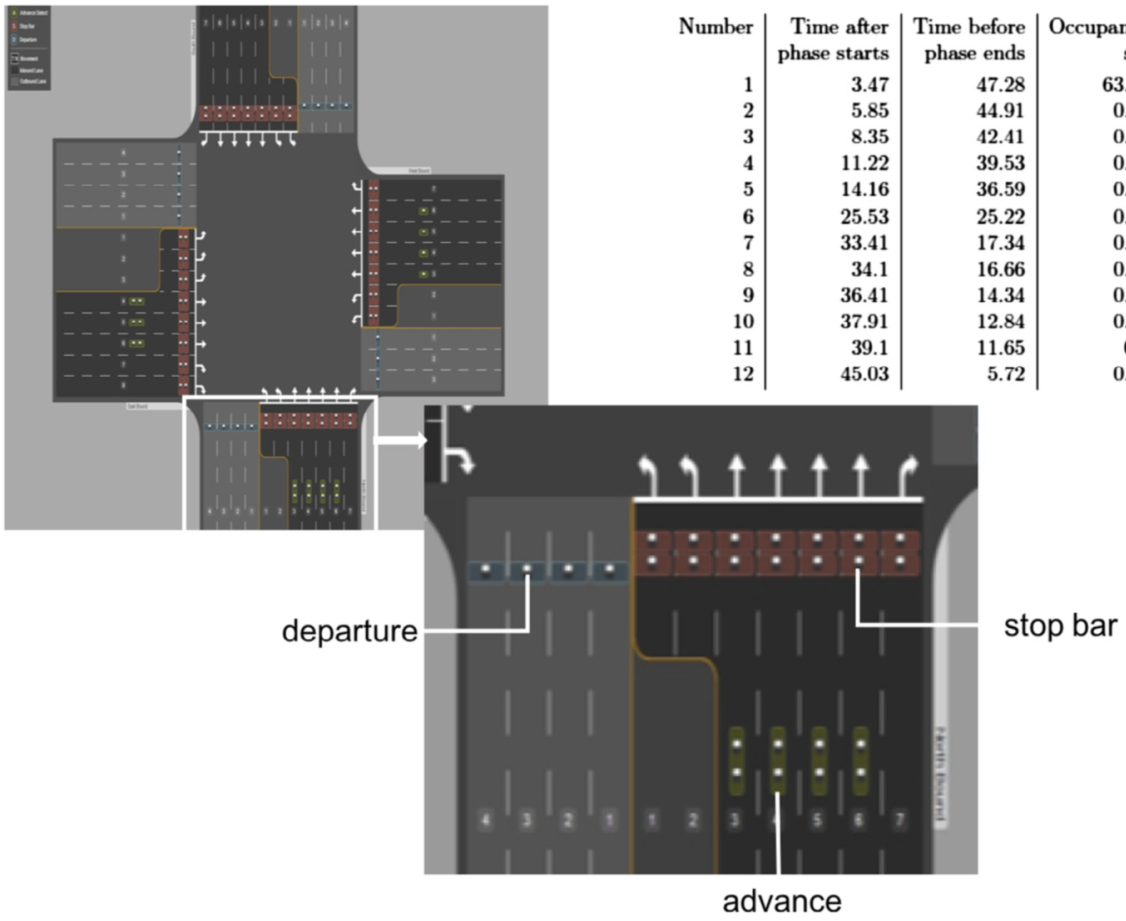

Number	Time after phase starts	Time before phase ends	Occupancy sec	Speed mph
1	3.47	47.28	63.88	17.53
2	5.85	44.91	0.44	28.33
3	8.35	42.41	0.81	33.43
4	11.22	39.53	0.81	24.52
5	14.16	36.59	0.56	33.53
6	25.53	25.22	0.31	52.75
7	33.41	17.34	0.44	52.75
8	34.1	16.66	0.38	52.51
9	36.41	14.34	0.56	40.93
10	37.91	12.84	0.56	52.75
11	39.1	11.65	0.5	40.93
12	45.03	5.72	0.12	73.72

Figure 1.3: Schematic of intersection detection system, and a trace of vehicles entering intersection from one through lane during one green phase.

= 1272 vph. Vehicles 5, 6, ... travel at much higher speed. Suppose these 12 vehicles were all to move as a platoon, that is, at the same speed of 45 mph (66 feet per second) with a uniformly small time headway of (say) 0.75 seconds (the space headway would be $0.75 \times 66 = 49.5$ ft), giving a saturation flow rate of $3600/0.75 = 4800$ vph, which is 3.8 times the observed rate of 1272 vph and 2.5 times HCM's theoretical rate of 1900 vph. The headways among vehicles $1, \ldots, 5$ are small, suggesting that they were queued at the stop bar. The larger headway between vehicles 6 and 7 and 7 and 8 suggests they were moving when the phase started. The small headway among vehicles $7, \ldots, 11$ suggest they were moving as a platoon. An estimate for an intersection with speed of 30 mph (44 feet per second) and a space headway of 40 feet is a (platoon) saturation flow rate of $(40/44) \times 3600 = 3960$ vph, which is twice HCM's 1900 vph and up to three times the rates observed in today's intersections. The following fact summarizes the relationship between platooning and the increase in saturation flow rates: **platooning decreases the headway of vehicles**

crossing an intersection by a gain factor Γ and increases the saturation flow rates of an intersection by the same factor Γ.

What does it take to organize a platoon? If each of the 12 vehicles queued at (or approaching) the intersection in Figure 1.3 could measure, say by radar, the relative distance and speed from the vehicle in front of it, its longitudinal motion could then be controlled by an adaptive cruise control (ACC) algorithm that would maintain a tight headway. If furthermore, these vehicles could communicate with each other and with the signal controller (for phase information), a cooperative adaptive cruise control (CACC) algorithm would maintain an even shorter headway and thus achieve a greater saturation flow rate.

Platooning is technically feasible. In fact, an autonomous 8-vehicle platoons with 16 ft gap traveling at 60 mph was demonstrated 20 years ago in 1997 by the National Automated Highway System Consortium [11, 43]. Since then vehicle automation has been greatly facilitated by advances in actuation (electronic braking, throttle, and steering) and sensing (radar and video), while platoon stability and control design are much better understood. Indeed, in [36] authors report an experiment of a 6-vehicle CACC platoon, with a 0.5 s headway. They used ACC equipped vehicles augmented with vehicle-to-vehicle (V2V) communications using a 802.11a WiFi radio in ad-hoc mode. Experiments with a 4-vehicle platoon, capable of cut-in, cut-out and other maneuvers, using CACC technology, are described in [28]. The vehicles' factory-equipped ACC capability was enhanced by a dedicated short-range communication (DSRC) radio that permitted V2V communication to enable CACC. The vehicles in the platoon had a time gap of 0.6 seconds (time headway of 0.8 seconds) traveling at 55 mph. ACC is today common in many high-end cars.

It is important to distinguish our proposal to use [C]ACC to increase an intersection's capacity from proposals to use [C]ACC to increase road capacity by decreasing headway. Increasing the capacity of urban roads will not increase the throughput of the urban network, which is limited by intersection capacity.

1.3 Objective

The aim of the current project was to develop a suite of techniques that will:

1. enable assessment of intersection efficiency;

2. model impact of [C]ACC on arterial traffic flow; and

3. make traffic on urban streets more reliable and predictable.

Working toward this goal, we delivered:

1. arterial measurement data collection system;

2. analysis of phasing and timing of actuated signals;

3. evaluation of car following models and their parameters;

4. model of ACC and CACC platooning in mixed traffic; and

5. micro-simulation model of signalized arterial network in Rollins Park, MD, built from measurement data.

1.4 Scope

The proposed techniques combine traffic management and traffic information.

Traffic management comprises feedback control of the road network infrastructure and demand management through traveler information, advisory messages and pricing. It happens on three levels:

1. at the vehicle level the car speed and headway are adjusted to increase throughput and safety;

2. at the road link level signal timings are optimized and special lanes re-allocated, e.g. bus lanes may be opened for everyone when necessary; and

3. at the network level traffic demand is managed via route advisory, day-to-day intersection timing adjustments, and traffic information dissemination.

Traffic information helps to provide reliable travel advice, assess the transportation system's performance, scenario analysis and future forecasts. It includes the current state of traffic and short term forecasts. It influences traveler departure times and route choices, as well as transportation modes. Traffic information is thus

a demand management tool, and its effectiveness depends on the accuracy of the information and the quality of the routing and transportation mode alternative advice provided to the travelers. Traffic information also enables one to assess the effectiveness of traffic management schemes.

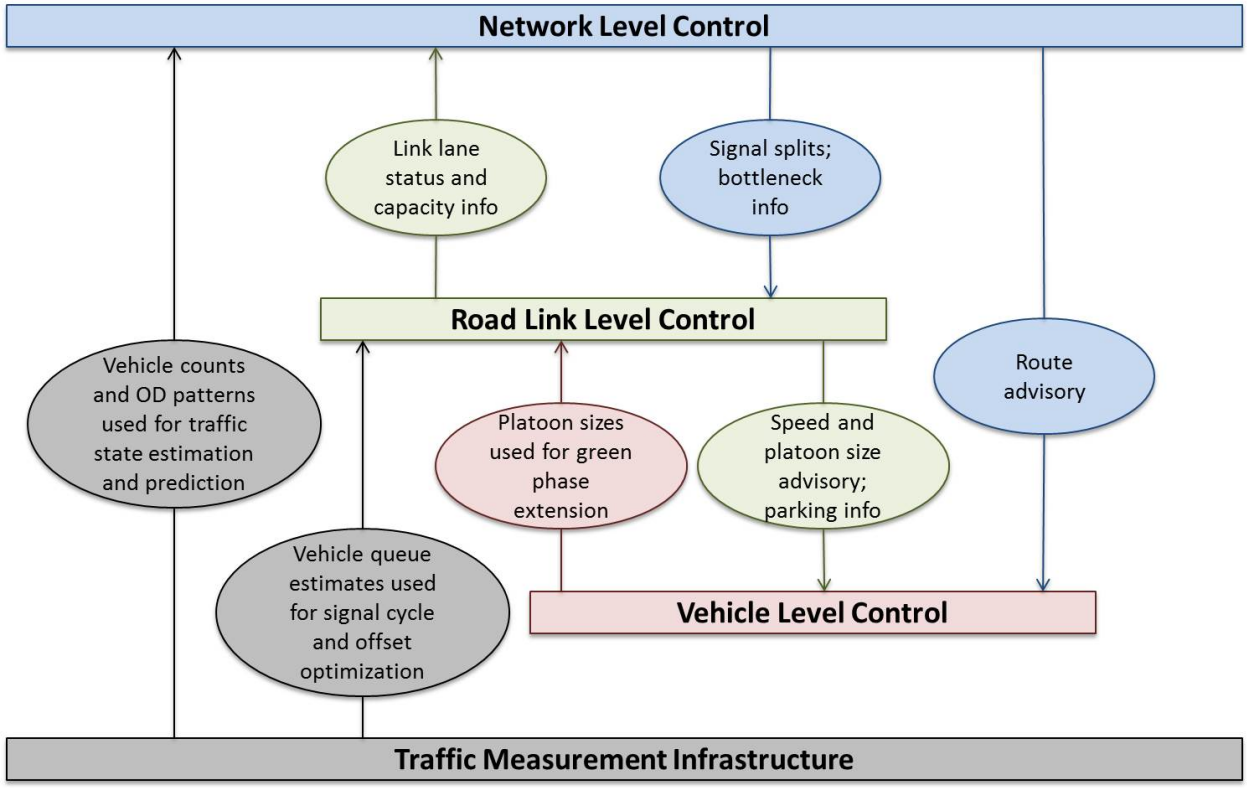

Figure 1.4: Information flow.

Figure 1.4 shows the information flow between the traffic measurement infrastructure and the proposed management layers. The vehicle level control system makes a group of connected vehicles move in a fuel efficient manner by reducing the number of stops at intersections. The flow through intersections is increased by forming platoons with minimal inter-vehicle spacing. The road link level control system includes signal timings that are tuned to increase traffic throughput. The goal is to improve the effective green (so that the green time is not wasted) and progression quality (so that most vehicles arrive at the intersection during green time). The lane management component aims to increase the link capacity at certain times of day by opening designated lanes to all the traffic. Sometimes, designated lanes may be used for parking. The network level control system determines intersection signal split timings to minimize congestion and delay. Signals are tuned to favor traffic on particular routes at a given time of day. This influences traveler route choices when reinforced by disseminating routing information.

Proper deployment and management of signalized intersections relies on the continuous process of:

1. obtaining and analyzing of signal phasing and traffic measurement data;
2. operations planning — simulating various scenarios, operational strategies as well as impact of new and emerging technologies in vehicles and multimodal transportation;
3. implementing the most promising operational strategies in the field.

This process requires a fast and trusted traffic simulator for the rapid quantitative assessment of a large number of operational strategies for the road network under various scenarios. The research presented hereby is the stepping stone for achieving this goal.

Chapter 2

Methodology

2.1 Research Setup

To perform this project, we chose a site with seven instrumented intersections, located in Rollins Park, Maryland. Intersection instrumentation is provided by Sensys Networks, Inc. (www.sensysnetworks.com). The site map is shown in Figure 2.1. In each of the seven locations counts of vehicles approaching the intersection, crossing stop bar and exiting the intersection, together with signal phasing data are collected. Signal phasing is important because all seven signals are actuated (as opposed to pre-timed): for a given approach, green time varies between minimum and maximum thresholds, getting extended beyond the minimum threshold as new vehicles arrive.

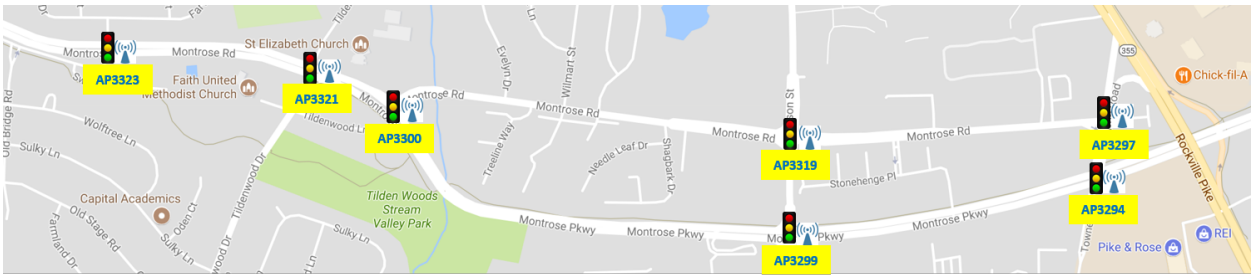

Figure 2.1: Map showing locations of seven instrumented intersections in Rollins Park, MD.

The diagram in Figure 2.2 depicts the process of data collection, analysis and building the simulation model. This diagram has six components, which we describe next.

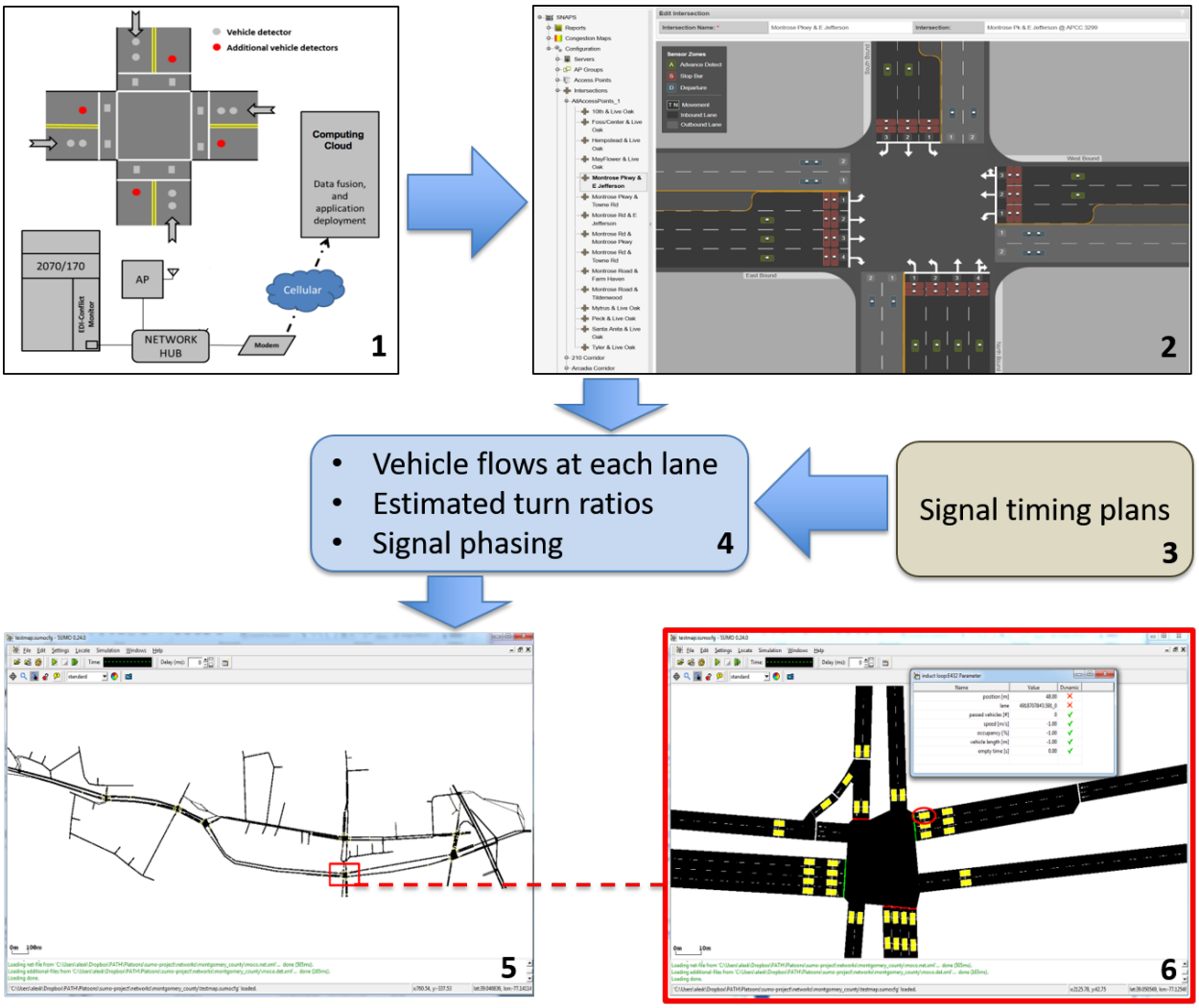

Figure 2.2: Process of data collection, analysis and building the simulation model.

1. The instrumentation of each intersection includes approach, stop bar and exit vehicle detectors; an access point (AP) that accumulates detector data to produce vehicle counts; and a conflict monitoring card that is installed together with the signal controller and records the information about signal phasing. The conflict monitoring card is connected to AP, which collects both vehicle counts and signal phasing. AP is equipped with cellular modem used to send the collected data to Sensys cloud for processing. For this project we set up a dedicated server that replicates those data sent by the seven APs to the Sensys cloud and stores them.

2. This component depicts intersection layout corresponding to AP3299, shown in Figure 2.1. Data collected from each intersection allows to analyze the performance of actuated signals and assess

intersection throughput.

3. Signal timing plans provide: cycle lengths, minimum and maximum green times for each phase and offsets specifying when a cycle at a given intersection starts relative to a global clock. Every phase corresponds to a movement, as shown in Figure 1.2. All this information is necessary for configuring signals in the simulation model.

4. Vehicle counts per lane at stop bar and exit detectors can be used to estimate turn ratios at intersections — in what proportion traffic breaks down into left turn, through movement and right turn. Signal timing plans and actual phasing data together with historical vehicle counts can be used to forecast signal behavior. All together, these data provide sufficient input for the simulation model.

5. We build a model of Rollins Park network for Simulation of Urban Mobility (SUMO) [25], a free, open source micro-simulation package. SUMO can be enhanced with custom models and provides various APIs to remotely control the simulation. This component shows a screenshot of graphical SUMO display.

6. If we zoom into the intersection corresponding to AP3299, the same as depicted by component 2, we can see that vehicle detectors modeled in the simulation exactly correspond to actual detectors deployed in the field.

Next, we discuss intersection data analysis.

2.2 Intersection Measurement Data Analysis

The analysis of intersection dataconducted in the current project focuses on signal phasing and timing (SPaT). SPaT refers to the current phase at a signalized intersection together with the residual time of the of the current phase for every approach to the intersection. The estimate is periodically broadcast by the intersection, say once per second. For a fixed-time controller the SPaT information will be definitive; the challenge is for an actuated controller for which only an estimate of the residual time can be given. A SPaT message is usually accompanied by a MAP message, which describes the physical geometry of one or more intersections. A vehicle approaching or departing the intersection can take the residual time of the

current phase from the SPaT message, together with knowledge of its own position and speed and MAP information, to calculate a speed profile that reduces stop-and-go driving and idling [49].

Several studies offer such 'eco-friendly' speed advice and simulate its benefits. In [3], authors use model predictive control (MPC) to construct a vehicle trajectory that traverses a sequence of intersections without stopping at a red light, knowing the signal phase timing sequence in advance. In [39], authors propose speed advice based on SPaT messages from the upcoming intersection and evaluate the expected reduction in emissions and fuel consumption using a vehicle dynamics model. In [7], authors simulate a velocity planning algorithm for eco-driving through a signalized corridor. These studies report fuel savings in arterial driving ranging between 12 and 47%. This wide variability in fuel savings estimates may be due to differences in the underlying vehicle simulation models.

On the other hand, the Glidepath field experiment found drivers who got speed advice saved 7%, whereas SPaT-based automatic speed control saved 22% of fuel, relative to an uninformed driver [48]. The Glidepath experiments suggest that accuracy in the SPaT estimate is essential to maximize the fuel savings that automation can achieve. Another field experiment [56] reports comparable fuel savings. For a review of the SPaT message structure and other SPaT applications see [34].

A few studies propose SPaT estimation based on poor measurements of signal phase. In [13], authors estimate the cycle length, phase durations, and the cycle start time for several intersections along a segment of Van Ness Avenue in San Francisco. Only fixed-time signals are considered. Their data consists of samples of GPS position and speed taken once every 20-80s from bus runs over this segment for one month. However, to estimate the red duration at an intersection, only between 40 and 350 samples out of 4,300 bus runs collected over one month were found to be usable. These few samples were "aggregated" (in an unspecified manner) to estimate the duration of red. The accuracy of the estimates is unimpressive, with absolute errors up to 7s for an average red duration of 35s. Since the signal timing parameters are fixed and available from the San Francisco Transportation Authority, the one month-long data collection and processing effort to estimate these parameters seems misspent. This approach to estimating parameters for fixed-time signals using speed measurements of "floating cars" was also used by [5, 52, 38].

In [24], authors describe an application in which several drivers with smartphones cooperate to find (detect) the signal light at an intersection and predict its phase duration. Much effort is spent to detect the signal

head and identify the signal color. (In the two reported scenarios, the signal head misdetection rates were 7.8 and 12.4%, meaning that in one out of ten intersections on average, the signal head was not detected or some other object was mistaken for a signal head.) The two remaining tasks are: (1) estimating the phase durations; and (2) 'synchronization' or locating the current time within the current cycle or phase, so the vehicle can figure out the residual time of the phase. In case of a fixed-time signal with known timing plan, the phase durations are known, and synchronization is achieved simply by determining the time of a phase transition from (say) green to red. For an actuated signal the phase duration varies from one cycle to the next, and three machine learning algorithms are tested to predict the duration of the next phase from signal phase history: however, the best prediction based on the five previous phases and cycle lengths is only slightly better than taking the next phase duration to be the same as the last duration. The authors do not discuss how phase duration estimates made by vehicles at earlier times are transferred to the vehicle that is making the current prediction.

These two studies spend much effort in collecting and processing noisy measurements of signal phase. By contrast, city transportation agencies and auto companies obtain the signal phase data directly from the signal controller. Cities may invest in SPaT devices to improve mobility generally and to provide priority to public transportation [31]. Auto companies devote their effort to improving SPaT algorithms and designing interfaces to present SPaT messages to drivers. The algorithm in [37], discussed in detail in the next section, predicts phase actuations during cycles $[t, t+d]$ based on measurements of signal phase during cycles $[t-2d, t-d]$. Here, d is the delay in acquiring phase information from the city. The brief description in [4] does not explain how their SPaT estimate is derived but states that it is displayed to the driver via a "countdown clock on the dashboard." The website (http://conectedsignals.com) states that its SPaT estimates combine real-time signal data, GPS location, and speed limit information, and are delivered via cellphones.

Report Contributions This report presents several algorithms to estimate the residual duration of a phase for a semi-actuated intersection in Rollins Park, MD. Direct measurements from the intersection are used to evaluate the algorithms. The algorithms predict the times for all future phase transitions, based on previous phase measurements and on the real time information that locates the current time within the current phase. For actuated signals, conditioning the prediction on this real time information greatly reduces the prediction error. To our knowledge, this is the first paper to use this information, which is available at the signal controller. A surprising finding is that for semi-actuated signals, as time increases, the estimate of

the residual phase duration may increase or decrease, posing a challenge to construct fuel-minimizing speed profiles. Another contribution stems from the observation that for a driver the best SPaT estimate is the one that minimizes the driver's own loss function. For example if, as seems likely, drivers differently weight errors in predicting 'end of green' and 'end of red', drivers on two different approaches would prefer different estimates of the same phase transition, since 'end of green' for one approach to the intersection would be the 'end of red' for the other. This suggests that multiple SPaT estimates should be created and broadcast.

This Section is organized as follows. Subsection 2.2.1 describes the intersection site and the measurement system. Subsection 2.2.2 formulates the SPaT estimation problem. Subsections 2.2.3 and 2.2.4 present three SPaT estimation algorithms.

2.2.1 Measurement Site

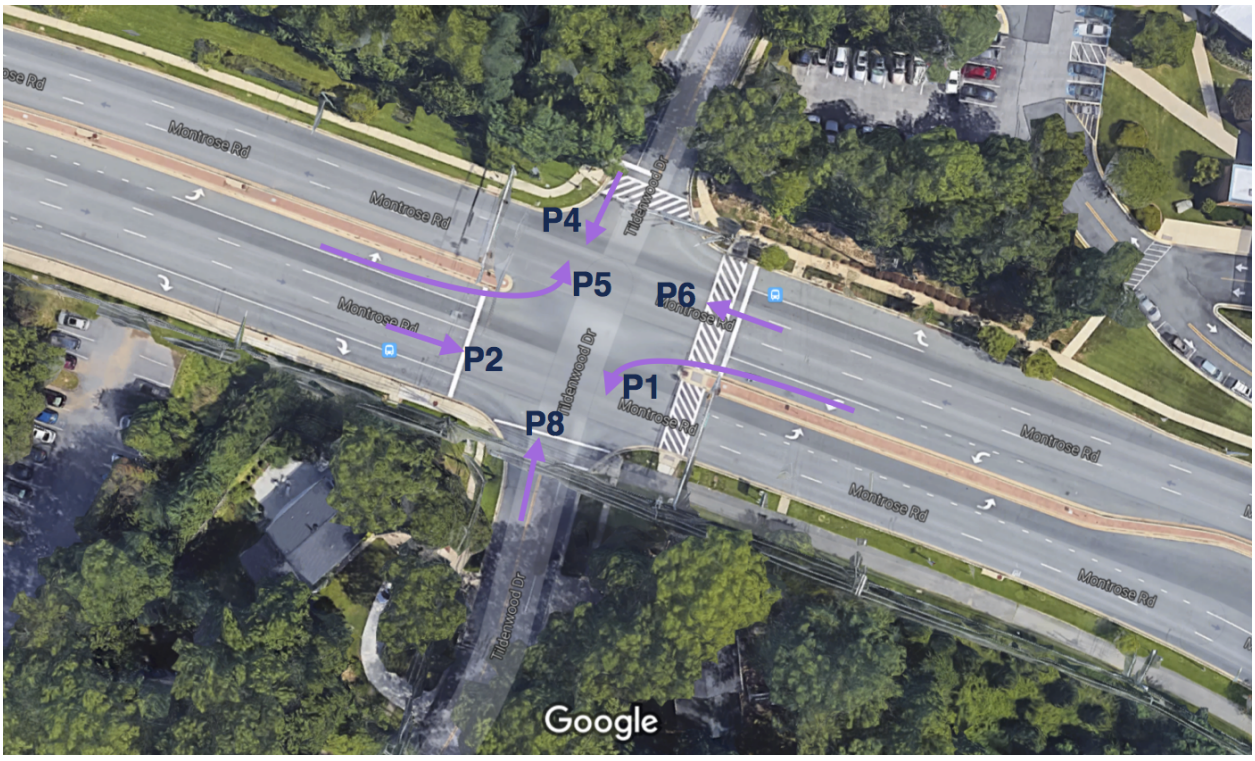

Figure 2.3: Intersection at Tildenwood Drive and Montrose Road

Figure 2.3 shows the intersection at Tildenwood Drive and Montrose Road in Rollins Park, MD (AP3321 in Figure 2.1), where all our data is collected. The same figure also indicates the six phase movements permitted at this intersection. The movements are arranged in the dual ring of Figure 2.4. Ring 1 comprises

phases p_4, p_1, p_2, and ring 2 comprises phases p_8, p_5, p_6; phases p_3, p_7 have zero duration. The thicker vertical lines are the two barriers. Across Montrose Rd., to the east of the intersection, is the pedestrian cross-walk which is actuated in every cycle at the beginning of phases p_4 and p_8.

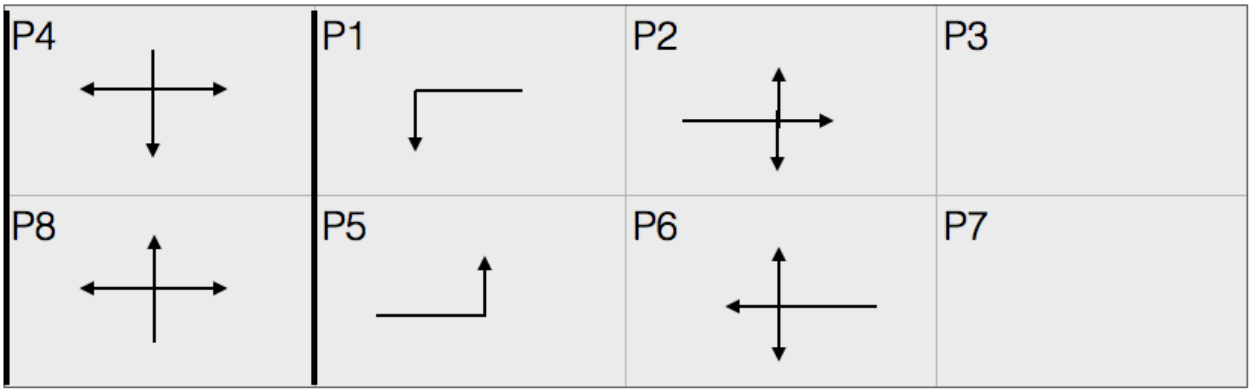

Figure 2.4: The dual-ring diagram; phases p_3 and p_7 have zero duration. The thicker vertical lines are the two barriers.

The intersection is equipped with magnetic vehicle detectors. There are detectors at the stop bar, at advance locations, and in the departure lanes. The latter permit an accurate count of turn movements (p_1 and p_5). In addition, the current signal phase is obtained from the controller every 100ms. All measurements are time stamped with a common clock with a 10ms accuracy. These detectors are for measurement only; the controller itself relies on different detectors for signal control.

In summary, the data consists of the time series of vehicle detections and signal phase at a time resolution of 10ms. The data is sent wirelessly to an access point (AP) mounted on a pole at the controller, from where it is sent via cellular connections to the traffic management center and to our server. The data are obtained courtesy of Sensys Networks, Inc. The analysis here uses one month of data for October 2015. *Only phase data is used in this study*; a future research will report on the additional predictive power provided by vehicle detection data.

The intersection is regulated by a semi-actuated, coordinated controller. The cycle length is fixed at $L =$ 100, 110 or 120s, depending on time of day and day of week. Phase p_4 or p_8 is the synchronizing phase, which starts each cycle. The cycle is divided into nominal durations for each phase; the controller modifies these durations in each cycle depending on vehicle detections. ([14] describes the operation of actuated

controllers.) The main direction of traffic is East-West and this direction has no detectors for signal control. There are detectors in the secondary North-South direction. If few vehicles are detected in the secondary direction, its green duration (phases p_4, p_8) is shortened and the time saved thereby is added to the green duration of the main direction (phases p_2, p_6). Vehicles making left turn movements (phases p_1, p_5) are also detected, and their green duration is also reduced if fewer vehicles are detected in the turn pockets, see Figure 2.3.

Thus if we denote by d_i the duration of phase p_i, we see that all of these durations may vary from one cycle to the next, while maintaining some identities:

$$d_4 + d_1 + d_2 = d_8 + d_5 + d_6 = L, \tag{2.2.1}$$

$$d_1 + d_2 = d_5 + d_6, \tag{2.2.2}$$

$$d_4 = d_8. \tag{2.2.3}$$

Equation (2.2.1) recognizes L as the cycle length; (2.2.2) and (2.2.3) are implied by the two barriers shown in Figure 2.4.

2.2.2 The Signal Phase and Timing (SPaT) Problem

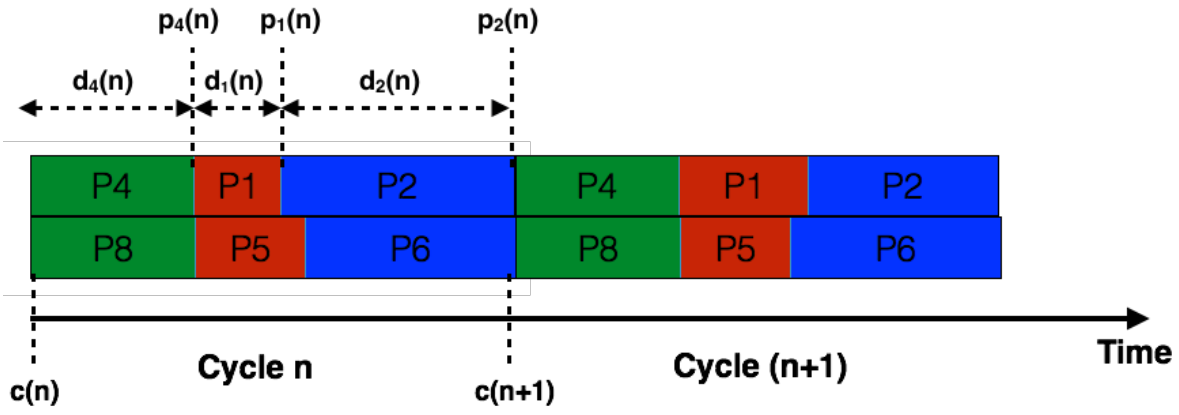

Figure 2.5: Variables used to define the SPaT estimation problem.

We use Figure 2.5 to define the SPaT estimation problem. Time is in seconds. The figure shows two

cycles n and $n+1$, each of length L, starting at times $c(n)$ and $c(n+1)$; $d_4(n), d_1(n) \cdots$ is the duration and $p_4(n), p_1(n), \cdots$ is the end time of phase $p_4, p_1, \cdots$ in cycle n; so if t is the current time in cycle n during phase $p_4, p_1, \cdots$, then $p_4(n)-t, p_1(n)-t, \cdots$ is the residual time of the phase that is included in the SPaT message. Observe that from the phase end times one can calculate the phase durations, e.g. $d_1(n) = p_1(n) - p_4(n)$, etc. Conversely, from the phase durations one can calculate their end times.

The SPaT Problem Let $I(t)$ be the information about previous phases available at time t during cycle n. The problem is to predict the residual times $p_k(m) - t$ of all phases k for all future cycles $m = n, n+1, \cdots$, given $I(t)$.

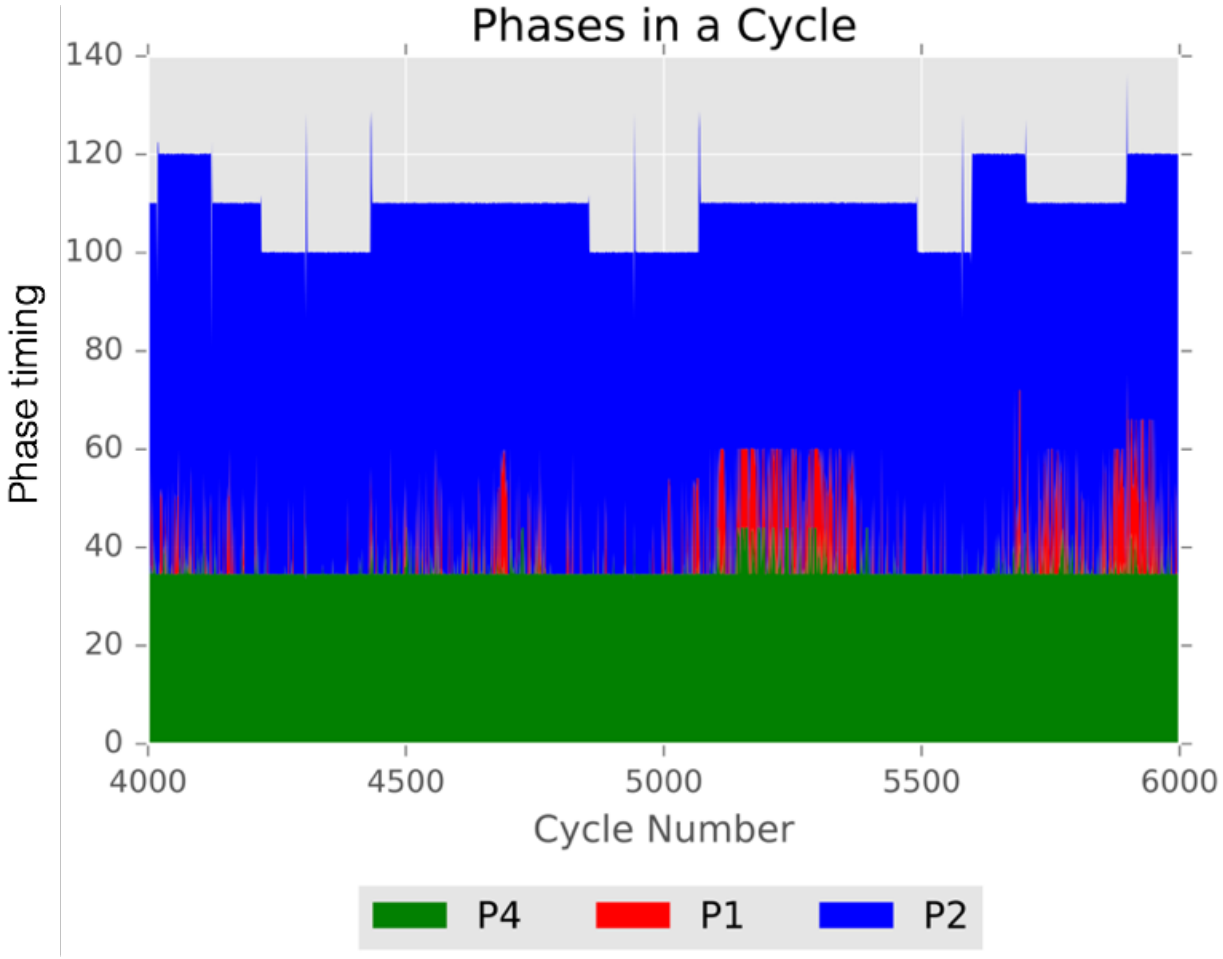

Figure 2.6: Variation in Phase durations over 2,000 cycles.

Our study uses data for 16,000 cycles in October 2016. The phase data for a sample of 2,000 cycles (about 3 days) is shown in Figure 2.6. The plot is similar to Figure 2.5: the difference is that the plot is rotated 90 degrees, the 2,000 cycles are 'stacked' horizontally, and only phases in ring 1 are shown (there is a similar

plot for phases in ring 2). The x coordinate is the cycle number; the y coordinate is the time in seconds during that cycle. The length of a cycle is 120, 110 or 100s, as determined by the timing plan. Every cycle starts in the synchronizing phase p_4 (and p_8); its duration is d_4 and it is colored green as in Figure 2.5. The minimum value of d_4 is the pedestrian clearance time of 36s; the duration d_4 (and d_8) is extended by 5s each time an additional vehicle is detected. Phase p_4 is followed by the left turn phase p_1 (and p_5) colored red, and lasting d_1. Duration d_1 depends on the detection of left turn vehicles, and each new detection triggers an extension of 5s. d_1 is zero in many cycles, when there are no left turns. The last phase in the cycle is p_2 (and p_6), colored blue. It lasts for time d_2 until the end of the cycle. Large values of d_4 and d_1 occur only during the AM and PM peaks. The 4s yellow and 1.5 or 2s red signal phases are included in the green duration.

We now present several algorithms for SPaT estimation.

2.2.3 The Approach of Protschky Et Al [37]

Suppose the data available at time t in cycle n comprises all the phase actuations that occurred during the d cycles $m \in (n-2d, n-d]$. This data can be put in the form of the binary array $g_k(i,m) = 1$ or 0, accordingly as phase k is or is not green (actuated) during second $i = 1, \cdots, L$ of cycle $m = n-2d+1, \cdots, n-d$. This data is used to predict future actuations during cycles $[n, n+d]$.

For each phase k, the data is 'compressed' into the frequency distribution $g_k(i)$ of actuations at second i of a cycle:

$$g_k(i) = \frac{1}{d} \sum_{m=n-2d+1}^{n-d} g_k(i,m),\ i = 1, \cdots, L. \tag{2.2.4}$$

We will evaluate (2.2.4) for that subset of the data of Figure 2.6 for which the cycle length is $L = 120$. (A separate analysis should be carried out for cycles of length 100, 110, as it makes no sense to combine these data.) The number d of such cycles is approximately 200. Using (2.2.4) gives the frequency distributions for phases p_4, p_1, p_2 shown in Figure 2.7. Also shown in the figure are two horizontal dashed lines corresponding to frequency 0.8 and 0.2; their significance will be discussed later.

The frequency distribution of phase p_4 has value 1 for the first 36s – the pedestrian clearance time – after which the the frequency declines until it reaches 0 at 44s into the cycle, and beyond which p_4 is never

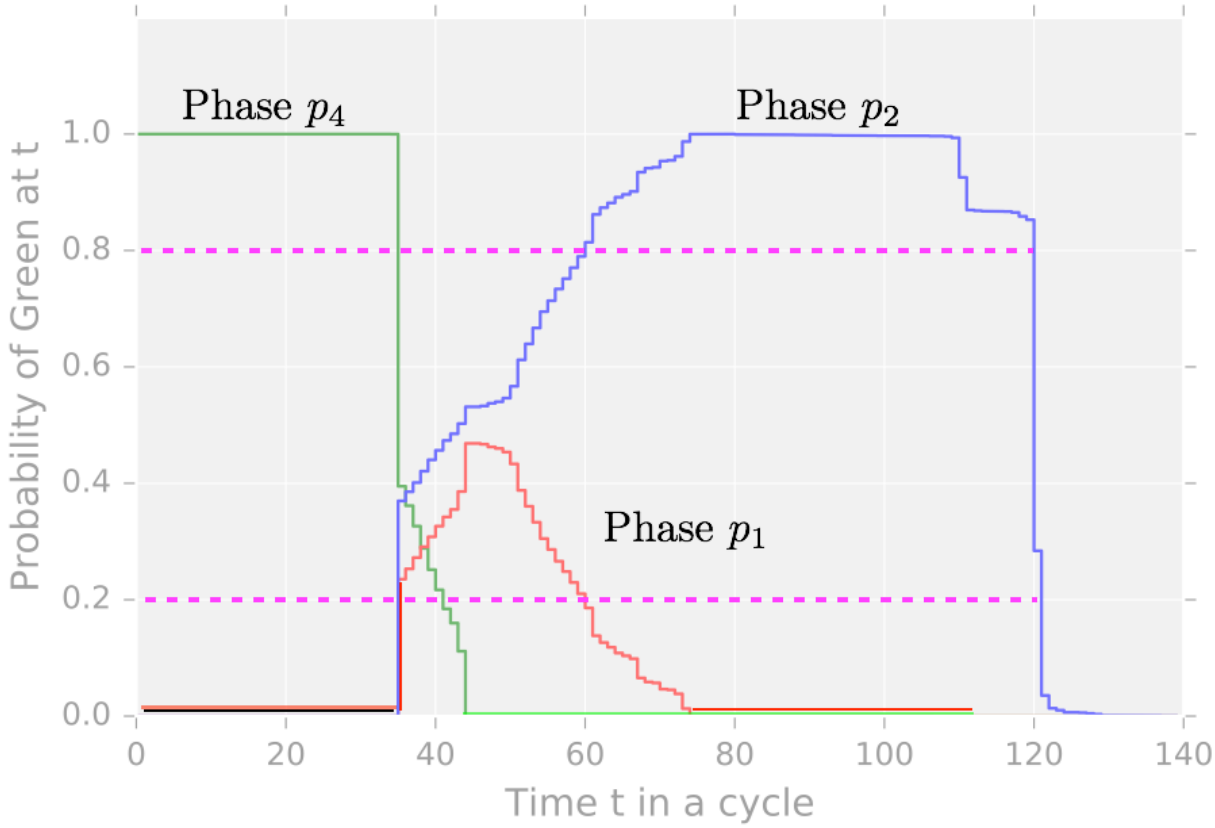

Figure 2.7: Frequency distributions for phases p_4, p_1, p_2 from data in Figure 2.6 for cycles of length 120s.

green. The frequency distribution of phase p_1 has value 0 for the first 36s (during which phase p_4 is always actuated) and then jumps to 0.2 at 36s, because there is a left turn movement in 20% of the cycle samples. The frequency of phase p_1 actuation increases up to 0.47 at 42s into the cycle, and then decreases to 0 at 73s into the cycle. (In Figure 2.6 one may observe that p_4 does last up to 73s during a few cycles of length 120s.) Lastly the frequency of phase p_2 being actuated is 0 until 36s, increases monotonically to reach 1 for seconds $i = 73, \cdots, 110$ and then declines to 0 at 120s, which is the end of the cycle.

The three frequency distributions can be expressed as L-dimensional vectors π_4, π_1, π_2 in which $\pi_k(i)$ is the frequency with which phase p_k is actuated during second i of the cycle. These frequencies are given by (2.2.4). Vectors π_8, π_5, π_6 are given by the same formula. The six vectors are not independent because of (2.2.1)-(2.2.3). (These vectors are *not* probability distributions, they simply give the frequency with which a phase is actuated during a particular second of the cycle.)

These six frequency distributions are computed at the beginning of each cycle when information about the

phase actuations of a new cycle is received. The computation can be done locally at each intersection, or it can be done centrally if local information is available at the traffic management center. [37] further compress the distribution from g_k of (2.2.4) to γ_k of (2.2.5):

$$\gamma_k(i) = \begin{cases} G, & g_k(i) \geq 0.8 \\ R, & g_k(i) \leq 0.2 \\ M, & \text{else} \end{cases} . \tag{2.2.5}$$

The interpretation of $\gamma_k(i) = G$ or R is that with 80% 'confidence' phase k is green or red at second i, whereas $\gamma_k(i) = M$ means the phase maybe green or red. In terms of Figure 2.7 $\gamma_k(i) = G$ or R accordingly as the distribution $g_k(i)$ is above the upper dashed line or below the lower dashed line; otherwise $\gamma_k(i) = M$.

In the scheme of [37], the intersection broadcasts the compressed versions (2.2.5) of the six distributions, say every second. But to figure out the residual time of the current or future phase, a vehicle also needs to know the broadcast time within the cycle. So we will assume that the SPaT message includes the time $t \in [1, 120]$ in the cycle when the broadcast is made, although [37] do not mention the need to broadcast this time. Even with this time, however, the vector γ given by (2.2.5) still may not be useful. Suppose, for example, a driver arriving at time 20s into the cycle wants to know when phase p_4 will end or when p_1, p_2 will start. From (2.2.5) and Figure 2.7 the answers will be: 'p_4 will likely end in 40-20 = 20s', 'no clue when p_1 starts', and 'p_2 will likely start in 60-20 = 40s'. Of course these '80% confidence' answers may be incorrect; and they leave a lot of uncertainty. A better response is provided in the next section.

The deeper problem with compressing the raw data of Figure 2.6 into the frequency distributions of (2.2.4) or Figure 2.7 is that the frequency distribution obscures the residual times of the phase, which is what the SPaT message is supposed to provide and vehicles need to calculate their speed profile. Consider a simple example to illustrate this. Suppose in an actuated signal with cycle length of 100s, one particular phase lasts exactly 20s in every cycle. Suppose further that the actuation of this phase can begin at any second i in the cycle with uniform probability, 0.01. So this phase will be actuated for an interval of 20s starting at any second in the cycle with uniform probability. Hence for this phase (2.2.4) gives $g(i) \equiv 0.2$ and (2.2.5) gives $\gamma(i) \equiv M$, and neither estimate conveys any information about this phase. On the other hand the same raw data implies that the duration of this phase is 20s with probability 1, which should be included in the SPaT message. Suppose further that the intersection knows the phase history up to the current time in the cycle.

In that case, the intersection knows that the phase was actuated (say) t seconds ago and so the residual time is exactly $20-t$. This message would be much more informative. We develop this idea next.

2.2.4 Residual Time Prediction

As in (2.2.1)-(2.2.3) and Figure 2.5, let d_4, d_1, d_2 denote the duration of phase p_4, p_1, p_2. (The treatment of phases p_8, p_5, p_6 is virtually the same.) Since in each cycle, each phase is actuated for a contiguous interval of time, it is easy to calculate the histograms or empirical probability distributions (pdf) of the durations from the raw data of Figure 2.6. Since $d_2 = 120-(d_4+d_1)$ (by (2.2.4)), it is enough to calculate the pdfs of d_4, d_1, d_4+d_1. Since d_4 and d_1 may be dependent, the pdf of d_4+d_1 cannot be calculated from the pdfs of d_4 and d_1. As in section 2.2.3 we consider only the data for cycles of length 120s. The calculated pdfs are plotted in Figure 2.8.

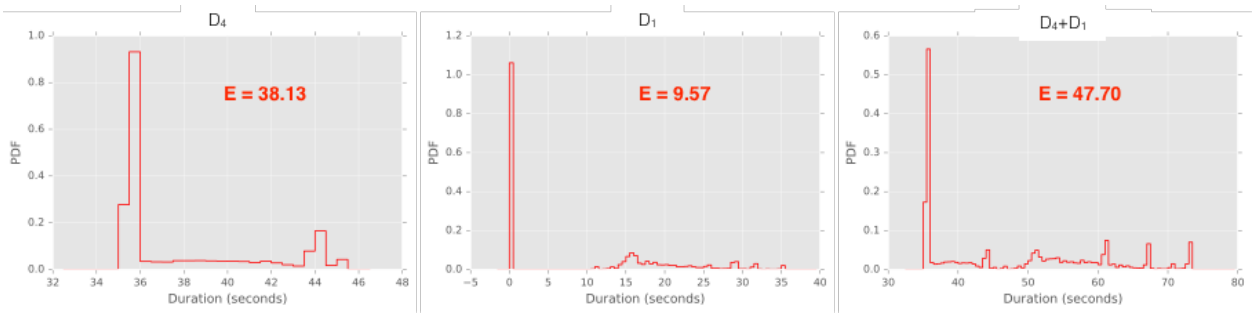

Figure 2.8: Pdfs for durations d_4, d_1, d_4+d_1 from data in Figure 2.6 for cycles of length 120s.

We propose several residual time predictors, depending on the information available at time t in the cycle that the prediction is made.

Conditional Expected Value as Prediction

If the prediction is made at the start of the cycle, $t=0$, then nothing is known except the unconditional pdfs of the phase durations in Figure 2.8, and so a reasonable prediction for the durations is their expected values. These values are inserted in the plots of Figure 2.8.

Now consider the prediction of the residual duration of d_4 at some later time t in the cycle. We see from the pdf of d_4 that if $t > 36$ and if the intersection knows that d_4 is still actuated at t, i.e., that $d_4 > t$, a better

prediction at t would be the expected value of d_4, conditioned on the event $\{d_4 > t\}$. The top right panel in Figure 2.9 shows the conditional pdf $p(d_4 \mid d_4 > 36)$ and its expected value 41.58. The bottom left panel plots the conditional expectation as a function of t, $t \mapsto E\{d_4 \mid d_4 > t\}$. The bottom right panel shows the prediction of the residual or the time remaining before the end of d_4, i.e., the plot of $t \mapsto E\{d_4 \mid d_4 > t\} - t$.

One striking feature is that the residual time of d_4 suddenly *increases* at $t = 36$ by about 2.5s, which may appear counter-intuitive. (Another consequence is that a driver waiting for the left turn signal, phase p_1, to turn green will see this time suddenly extended by 2.5s. The phenomenon is similar to the experience of the 'remaining time' to download a file.) If the residual time is revealed to the driver via a countdown clock as in [4], then the clock must make a backward jump at $t = 36$. By assuming that the prediction of the duration does not change with time, i.e., $E\{d_4 \mid d_4 > t\} - t = E\{d_4\} - t$, the eco-driving control strategies in [7] and [39] rule out the realistic situation depicted in the bottom right panel of Figure 2.10. Of course the complexity of Figure 2.9 disappears in the case of fixed-time signals, for which the pdfs are delta-functions.

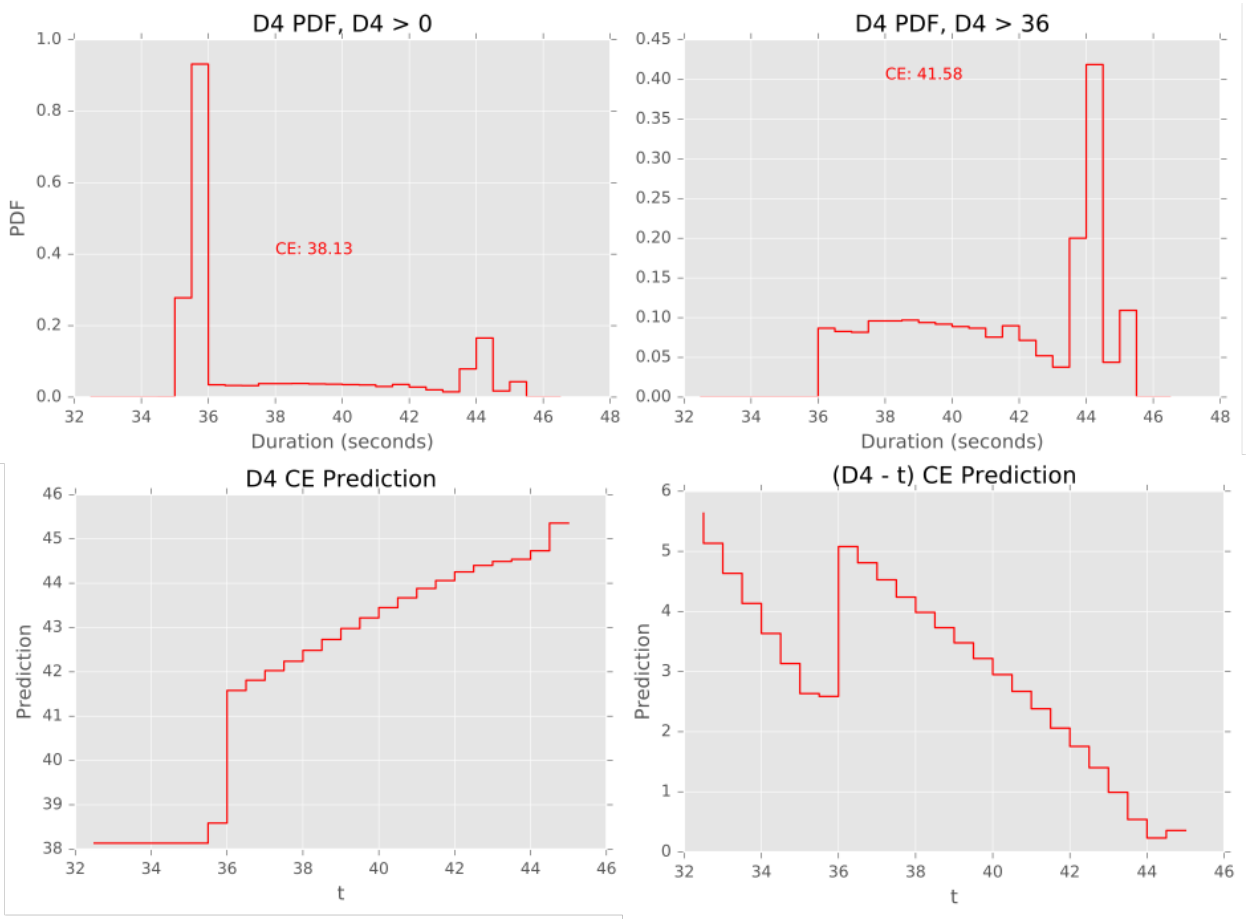

Figure 2.9: Unconditional and conditional pdfs for d_4, expected value and residual expected value.

Confidence Based Prediction

Suppose we want to provide a confidence bound on the predictions of the residual duration in the spirit of [37]. One way is to pick a confidence bound, say 0.3, and ask: For what value d can one guarantee $P\{d_4 > d\} = 0.3$? Let $F(d) = P\{d_4 \leq d\}$ be the cumulative distribution function (cdf) of d_4. Then $1 - F(d) = P\{d_4 > d\}$ and the answer to the question is given by the unique solution d of

$$1 - F(d) = 0.3. \tag{2.2.6}$$

The left panel of Figure 2.10 plots the pdf and 1-CDF of d_4. The latter is a decreasing function, and the solution of (2.2.6) is $d = 38$. Now suppose we ask the same question at time $t = 36$ into the cycle with p_4 actuated. Then the answer is given by

$$1 - F(d \mid d_4 > 36) = 0.3. \tag{2.2.7}$$

which yields $d = 43$. Here $F(d \mid d_4 > 36)$ is the CDF of d_4 conditioned on the event $\{d_4 > 36\}$. Thus with probability 0.3, at time $t = 0$ in the cycle d_4 is at least 36, and at time $t = 36$ in the cycle d_4 is at least 43.5. Evidently, having real-time information significantly improves the prediction, both in the form of conditional expectation (Figure 2.9) and with confidence bounds (Figure 2.10).

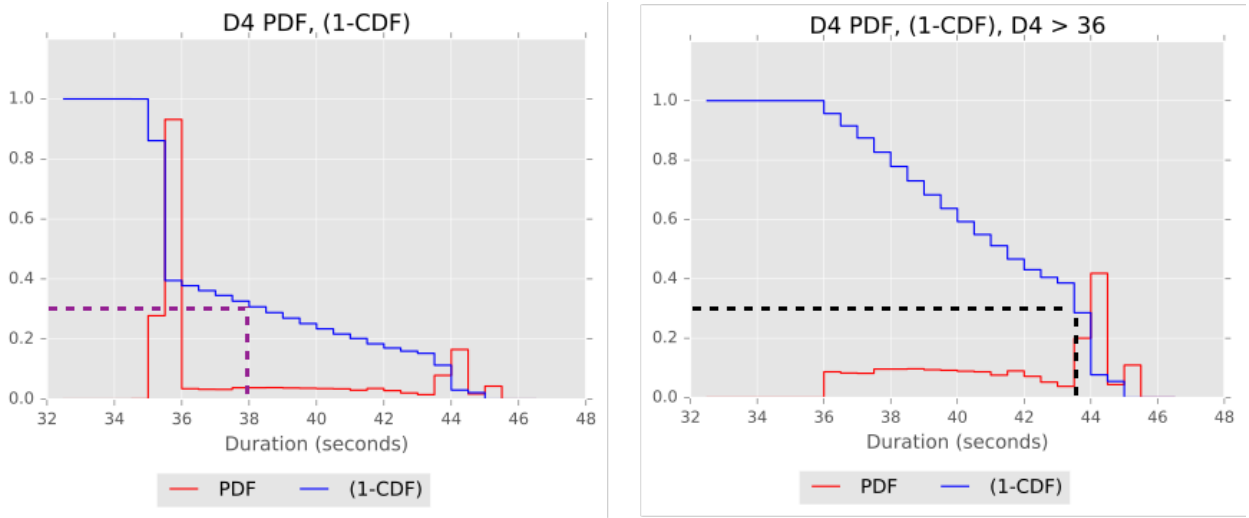

Figure 2.10: Left: $P\{d_4 > d\} = 0.3$ is $d = 38$. Right: $P\{d_4 > d \mid d_4 > 36\}$ is $d = 43.5$.

Observe that in (2.2.7), (2.2.10) the answer d is just the 0.7th quantile of d_4.

2.2.5 Prediction Errors

Consider the conditional expected value estimate of the bottom left panel of Figure 2.9 at time t into the cycle, for which the prediction of the residual time is $P(t)$. (For example, for $t = 42$, $P(t) = 44$.) In our data set there are several samples for which $d_4 > t$ and for each of those samples we can calculate the exact error in the prediction of the residual time, $P(t) - d_4$. We can then calculate the mean absolute error for the prediction at t:

$$MAE(t) = \frac{1}{n(t)} \sum_{\omega=1}^{n(t)} |P(t) - d_4(\omega)| \tag{2.2.8}$$

in which $\omega = 1, ..., n(t)$ are the samples of d_4 for which $d_4(\omega) > t$.

In exactly the same way we can calculate the MAE for confidence-based prediction shown in Figure 2.10. The formula for MAE is exactly the same as in (2.2.10), the only difference is that $P(t)$ is now the confidence-based estimate.

Figure 2.11 plots the the conditional expectation and confidence-based predictions and the prediction errors. The confidence bound is 0.3. The most remarkable aspect of the figure is that both prediction errors decrease as more real-time information is accumulated by the intersection.

If we take a quadratic loss function, (2.2.10) must be replaced by the mean-squared error (2.2.9):

$$MSE(t) = \frac{1}{n(t)} \sum_{\omega=1}^{n(t)} [P(t) - d_4(\omega)]^2 \tag{2.2.9}$$

in which $\omega = 1, ..., n(t)$ is the same as in (2.2.10). The best prediction error is now simply the conditional expectation.

2.2.6 Different Loss Functions

The function *MAE* in (2.2.10) implicitly takes the loss of an inaccurate prediction as the absolute value of the error, hence a positive error and a negative error of the same magnitude are judged equally. But it seems more likely that an over estimate of the 'time to red' is evaluated differently from the same error in the

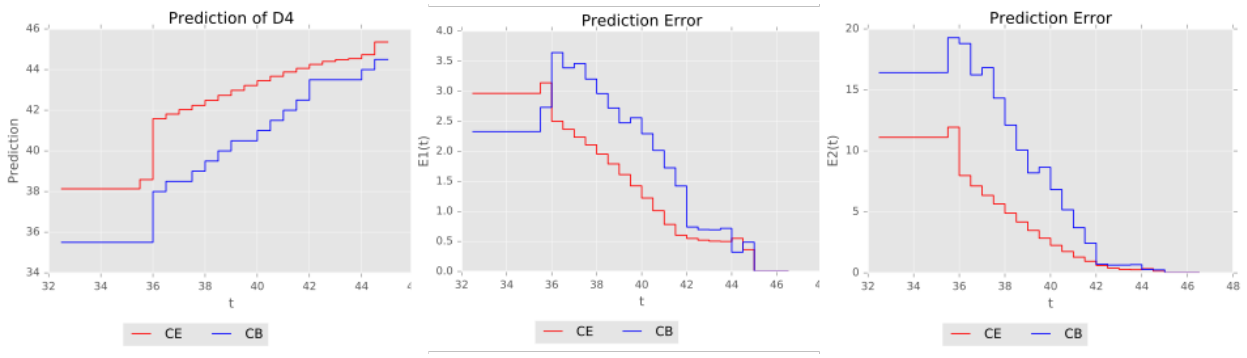

Figure 2.11: Left: Two predictors, middle: MAE errors for both predictors: conditional expectation and confidence-based as a function of observation time t; Right: MSE for both predictors.

estimate of 'time to green'. (In the former case, one may have to slam on the brakes.) This consideration suggests using the loss function

$$E[L(p-x)] = \int_0^p c_2(p-x)f(x)dx + \int_p^M c_1(p-x)f(x)dx. \tag{2.2.10}$$

Here c_2 is the cost per second of underestimation, c_1 is the cost per second of overestimation of the phase duration, p is the prediction, x is the actual duration, and $EL(p-x)$ is the expected loss. The best prediction that minimizes (2.2.10) is given by p^* where

$$F(p^*) = \frac{|c_1|}{|c_1+c_2|} \tag{2.2.11}$$

i.e. p^* is just the $|c_1|/|c_1+c_2|$th quantile of the duration. So this is just the confidence based estimate with an appropriate choice of the confidence bound.

This loss function is plotted in Figure 2.12. If $|c_1| \neq |c_2|$, the two slopes are different. So, if our driver feels $|c_1| < |c_2|$ when driving during phase p_2, he will feel the two slopes should be exchanged when driving during phase p_4.

2.2.7 Summary

We presented three algorithms for SPaT predictions, i.e., estimates of the remaining duration of a signal phase. The investigation is based on high-resolution phase data for a semi-actuated intersection in Rollins

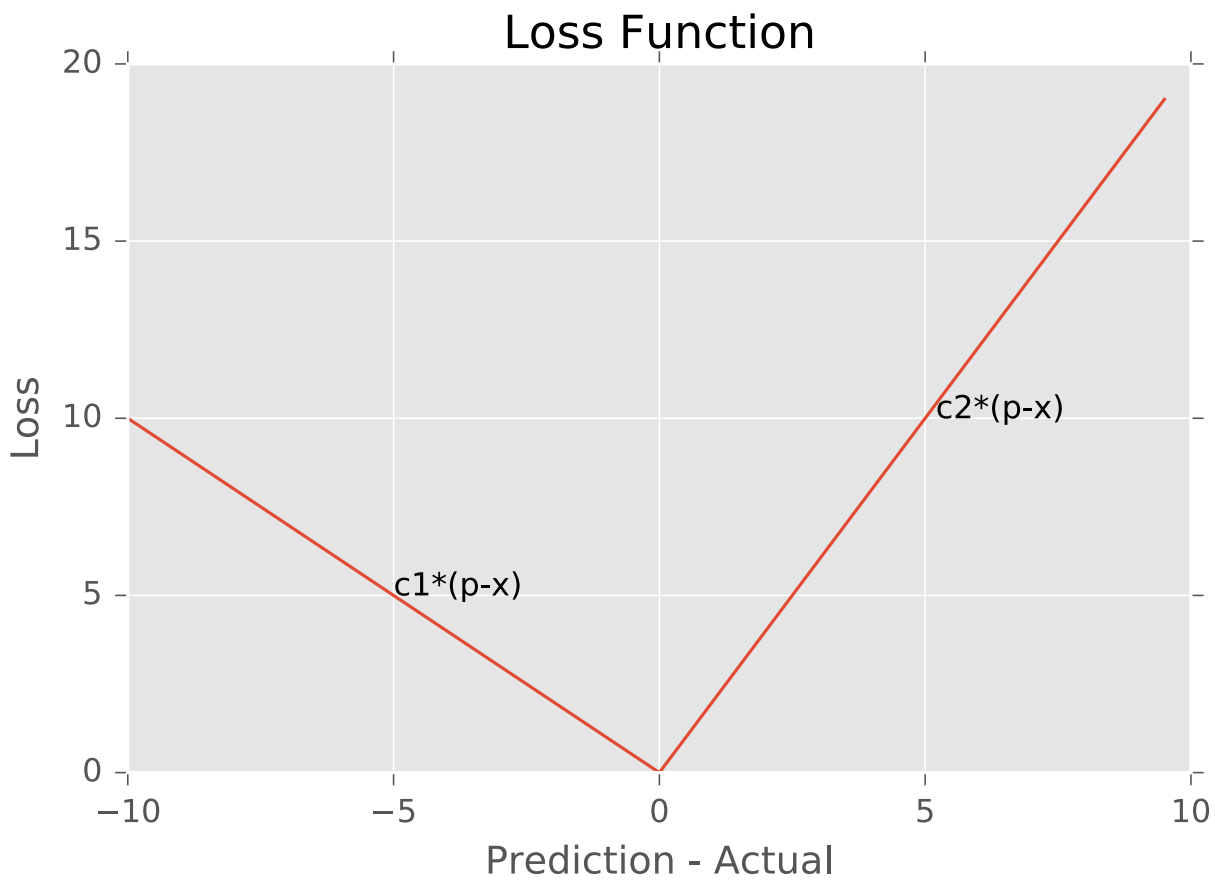

Figure 2.12: Left: Two predictors, middle: MAE errors for both predictors: conditional expectation and confidence-based as a function of observation time t; Right: MSE for both predictors.

Park, MD. In each case the prediction is calculated from the ground truth. The algorithms can be readily implemented at the intersection's signal controller. We summarize three principal findings.

First, having knowing in real-time how much time into the current phase has elapsed, greatly improves the prediction of the residual time for that phase and for a subsequent phase. Second, for an actuated signal, it is very likely that as time increases, the real-time prediction of the residual time can increase and decrease. This poses a challenge to the design of speed profiles that reduce fuel consumption. Third, drivers are likely to weight differently errors in predicting end of green and end of red, so drivers on two different approaches would prefer different estimates of the residual time of the same phase. It may be worth considering providing multiple estimates of the residual time.

Next, we discuss arterial traffic modeling.

2.3 Traffic Modeling

To assess the impact of ACC and CACC vehicles on intersection throughput, one has to model car following behavior. The choice of the car following models largely determines the findings of of the ACC/CACC impact study. There is a variety of car following models. The list starts with the Reuschel [40] and Pipes [35] models, in which the speed changes instantaneously as a function of the distance to the leading vehicle. Another class of models, generally referred to as Gazis-Herman-Rothery (GHR) [10, 17],[1] is where the acceleration depends on speed difference and the distance gap according to the power law and not influenced by the driver's own speed. These models are incomplete in the following sense: they can describe either free traffic or approach to standing obstacle, but not both. On the contrary, *complete* models describe all situations, including acceleration and cruising in free traffic, following other vehicles in stationary and non-stationary situations, and approaching slow or standing vehicles, and red lights [46] (Chapter 10).

The class of models, where the acceleration depends on speed difference with car in front and on the difference between the actual and the desired gap linearly, is attributed to Helly [20]. Helly modl is complete, and its linear nature makes it easy to understand and analyze. It was extensively studied, built upon and used for ACC/CACC modeling [44, 19, 51, 21, 50].

Another example of a complete model is the Optimal Velocity Model (OVM) [6]. In OVM, acceleration depends only on the distance (but not on the speed difference) to the car in front: this distance determines the optimal speed, which the vehicle tries to hold. OVM is not always collision-free. Full Velocity Difference Model (FVDM) [22] extends OVM by adding the linear dependence on the speed difference with the car in front to the acceleration equation. Generally considered more realistic than OVM, in terms of acceleration values and the shock waves that it produces, FVDM suffers from the defect that it is not complete in the sense defined above. The reason is that the speed difference term does not depend on the gap between the vehicle and the car in front. Consequently, a slow vehicle triggers a significant deceleration of its follower even if it is miles away. Newell car following model [32, 33], describes car-following behaviour based on the analysis of time-space trajectory, assuming that the time-space trajectory for two adjacent vehicles is essentially the same, except for the shift in time and space. For gaps smaller than desired and triangular fundamental diagram, the Newell model behaves the same OVM.

[1] Also known as General Motors car following model.

All the above mentioned models are heuristic — they attempt to describe vehicle flow based on observations and common sense. Gipps car following model [18] and the Intelligent Driver Model (IDM) [45] are similar to complete heuristic models in that they too are defined by their acceleration equations. In addition to that, they adhere the following principles:

1. the model is complete in the sense of the definition above;
2. the equilibrium gap to the car in front is no less than the *safe distance* computed as a sum of the minimal gap and the distance the car can travel during the period called reaction time;
3. deceleration increases and decreases smoothly under normal driving conditions, but can exceed "comfortable" level when the car in front is too close and too slow — to avoi collision;
4. transitions between different driving modes are smooth;
5. each model parameter describes only one aspect of driving behavior;
6. acceleration is strictly decreasing function of the speed;
7. acceleration is increasing function of the gap between the vehicle and the car in front;
8. acceleration is an increasing function of the speed of the car in front;
9. minimal gap to the car in front is maintained even during standstill, but there is no backward movement if the gap is smaller than the minimal (e.g. due to initial conditions).

Gipps model is widely used and is implemented in the Aimsun microsimulator. Krauss car following model [26] is a stochastic variation of Gipps model, where an auto-correlated noise is added to the vehicle speed. Krauss-Gipps model is implemented in the SUMO microsimulator [25]. IDM is considered to have more realistic acceleration profile than that of Gipps model. It is widely investigated for the purpose of ACC/CACC implementation [23, 41, 53, 28]. Due to the continuous transition between free flow and congested traffic, the gap between vehicles grows infinitely large as the speed approaches the equilibrium value. The other effect of this continuous transition is that the gap size between the vehicle and the car in front smaller than desired leads to unrealistically high deceleration values. This produces unacceptable vehicle behavior in platoons. Therefore, the acceleration function was modified to retain the spirit of IDM

but to eliminate its shortcomings. The resulting model is called Improved IDM (IIDM) [46] (Chapter 11). Gipps model and IIDM are sometimes called first *principle models*, referring to the four principles stated above.

Finally, there is a category of car following models referred to as *behavioral*. These are Wiedemann [54, 55] and Fritzsche [16] models, implemented in Planung Transport Verkehr (PTV) Vissim and Paramics simulators respectively. These two models are essentially hybrid systems, where guards between different modes of vehicle dynamics are thresholds for the speed difference and the distance to the car in front. Adjusting those guards changes driver behavior in the range from overly cautious to aggressive and from slow reactive to fast. In the Wiedemann and Fritzsche models, transitions between different driving modes are not necessarily smooth, as acceleration changes in a series of discrete transitions, which violates rule 4 of the first principles listed above. Designed to model human behavior and requiring complex tuning of the multitude of parameters, these models are generally not used for ACC/CACC.

In this report we analyze three models — Gipps, IIDM and Helly — and assess the impact of ACC and CACC vehicles on the intersection throughput in the context of these models.

2.3.1 Analysis of Selected Car Following Models

We start by introducing the notation that will be used in the car following model discussion. It is summarized in Table 2.1 together with the default parameter values that we will use in our experiments, unless stated otherwise.

The state update equations for a car following model are:

$$v(t+\Delta t) = v(t)+a(t)\Delta t; \tag{2.3.1}$$

$$x(t+\Delta t) = x(t)+\frac{v(t)+v(t+\Delta t)}{2}\Delta t = x(t)+v(t)\Delta t+\frac{a(t)\Delta t^2}{2}, \tag{2.3.2}$$

where acceleration $a(t)$ depends on the car following model — Gipps, IIDM and Helly — whose descriptions follow.

Symbol	Description	Default value
l	Vehicle length.	$l = 5$ m.
t, Δt	Time and the model time step.	$\Delta t = 0.05$ s.
$x(t)$	Vehicle position.	
$x_l(t)$	Position of the vehicle in front, the *leader*.	
$v_{\max}$	Maximal admissible speed for the vehicle.	$v_{\max} = 20$ m/s.
$v(t)$	Vehicle speed.	
$v_l(t)$	Speed of the leader.	
$a(t)$	Vehicle acceleration.	
$a_{\max}$	Maximal vehicle acceleration.	$a_{\max} = 1.5$ m/s^2.
b	Desired vehicle deceleration.	$b = 2$ m/s^2.
$g(t)$	Gap: distance from the front of the vehicle to the tail of the leader, $g(t) = x_l(t) - x(t) - l$.	
$g_{\min}$	Minimal gap that is allowed between the vehicle and the leader.	$g_{\min} = 4$ m.
$g_d(t)$	Desired gap between the vehicle and the leader.	
τ	Reaction time to decelerate for the vehicle to avoid collision with the leader.	$\tau = 2.05$ s.
$\theta(t)$	Headway: $\theta(t) = \frac{x_l(t)-x(t)}{v(t)}$.	
$f(t)$	Vehicle flow: $f(t) = \frac{1}{\theta(t)}$.	

Table 2.1: Notation for car following models.

- Gipps model:

$$a(t) = \min\left\{a_{\max}, \frac{v_{\max} - v(t)}{\Delta t}, \frac{1}{\Delta t}\left(-v(t) - b\tau + \sqrt{(b\tau)^2 + (v_l(t))^2 + 2b\,(g(t) - g_{\min})}\right)\right\}. \quad (2.3.3)$$

- IIDM:

$$a(t) = \begin{cases} a_{\max}\left(1 - \left(\frac{g_d(t)}{g(t)}\right)^{\delta_1}\right), & \text{if } \frac{g_d(t)}{g(t)} > 1; \\ a^*(t)\left(1 - \left(\frac{g_d(t)}{g(t)}\right)^{\delta_1 a_{\max}/a^*(t)}\right), & \text{otherwise,} \end{cases} \quad (2.3.4)$$

where

$$a^*(t) = a_{\max}\left(1 - \left(\frac{v(t)}{v_{\max}}\right)^{\delta_2}\right), \quad (2.3.5)$$

$$g_d(t) = g_{\min} + \max\left\{0, v(t)\tau + \frac{v(t)(v(t) - v_l(t))}{2\sqrt{a_{\max} b}}\right\}, \quad (2.3.6)$$

and δ_1, δ_2 are some fixed positive parameters.[2]

[2]In the original descriptions of IDM and IIDM, parameter δ_1 at $\delta_1 = 2$, but we believe, it does not have to be restricted to a

- Helly model:

$$a(t) = \min\left\{a_{\max}, \frac{v_{\max} - v(t)}{\Delta t}, \alpha_1\left(v_l(t) - v(t)\right) + \alpha_2\left(g(t) - g_{\min} - v(t)\tau\right)\right\}, \tag{2.3.7}$$

  where α_1 and α_2 are some positive fixed parameters.[3]

In all three models, the equilibrium speed ($a(t) = 0$) is achieved with $v(t) = v_l(t) = v_{\max}$ and $g(t) = g_{\min} + v(t)\tau$. In this case, equilibrium headway is:

$$\theta_e = \tau + \frac{g_{\min} + l}{v_{\max}}. \tag{2.3.8}$$

Assuming default values from Table 2.1, the length of the car $l = 5$ m, the speed limit $v_{\max} = 20$ m/s, the minimal gap $g_{\min} = 4$ m and the reaction time $\tau = 2.05$ s, from (2.3.8) we get $\theta_e = 2.5$ s,[4] which translates to $f_e = 1/\theta_e = 0.4$ vehicles per second, 24 vehicles per minute, or 1440 vehicles per hour.

Now let us compare the behavior of these car following models in three experiments with intersections. In these experiments we will be using the parameter values from Table 2.1, and specific IIDM and the Helly model parameters given in Table 2.2.

$\delta_1 = 8$
$\delta_2 = 4$
$\alpha_1 = 0.5$
$\alpha_2 = 0.25$

Table 2.2: Parameter values used for IIDM and the Helly model.

Experiment with a free road ahead.

Consider a setup presented in Figure 2.13.

The initial condition at time $t = 0$ is that infinite number of vehicles are standing in the queue with the minimal gap between them. The light turns green, and vehicles are released.

Figure 2.14 shows trajectories, speeds and accelerations of the first ten vehicles from the queue computed by the three car following models. The signal is located at position 0 indicated by the horizontal black line

given value.

[3] Helly determined that α_1 should be in the range $[0.17, 1.3]$, and α_2 could be selected in the range $\left[\frac{1}{4}\alpha_1, \frac{1}{2}\alpha_1\right]$ [9].

[4] Empirical evidence suggests that 2.5 seconds is a typical headway observed in dense traffic on urban streets.

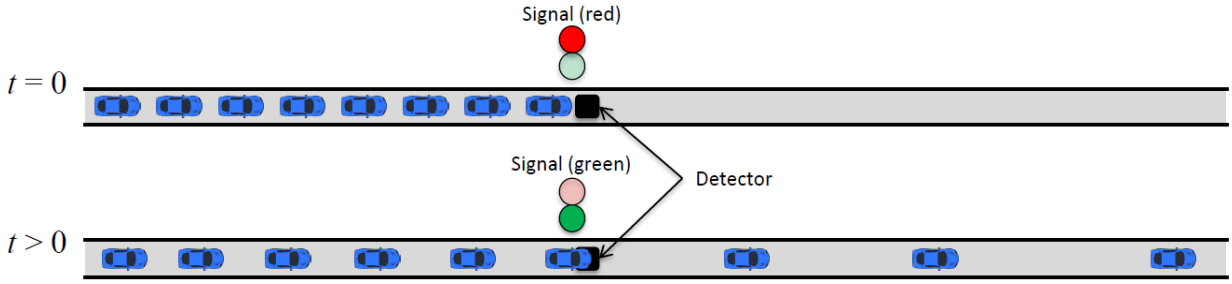

Figure 2.13: Signal turns green at time $t = 0$, and vehicles start moving. The first vehicle has free road ahead.

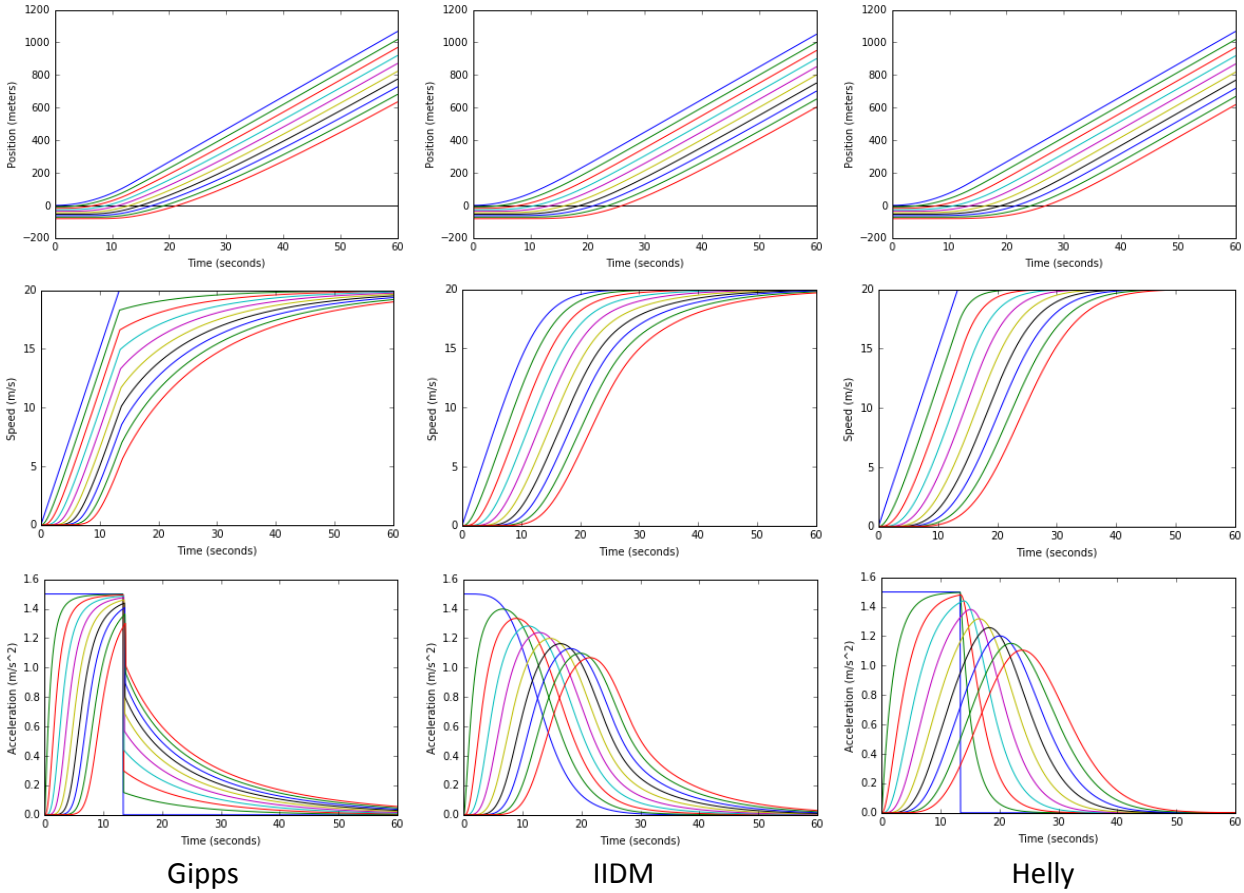

Figure 2.14: Experiment with a free road ahead: comparison of vehicle trajectories, speeds and accelerations between the three car following models.

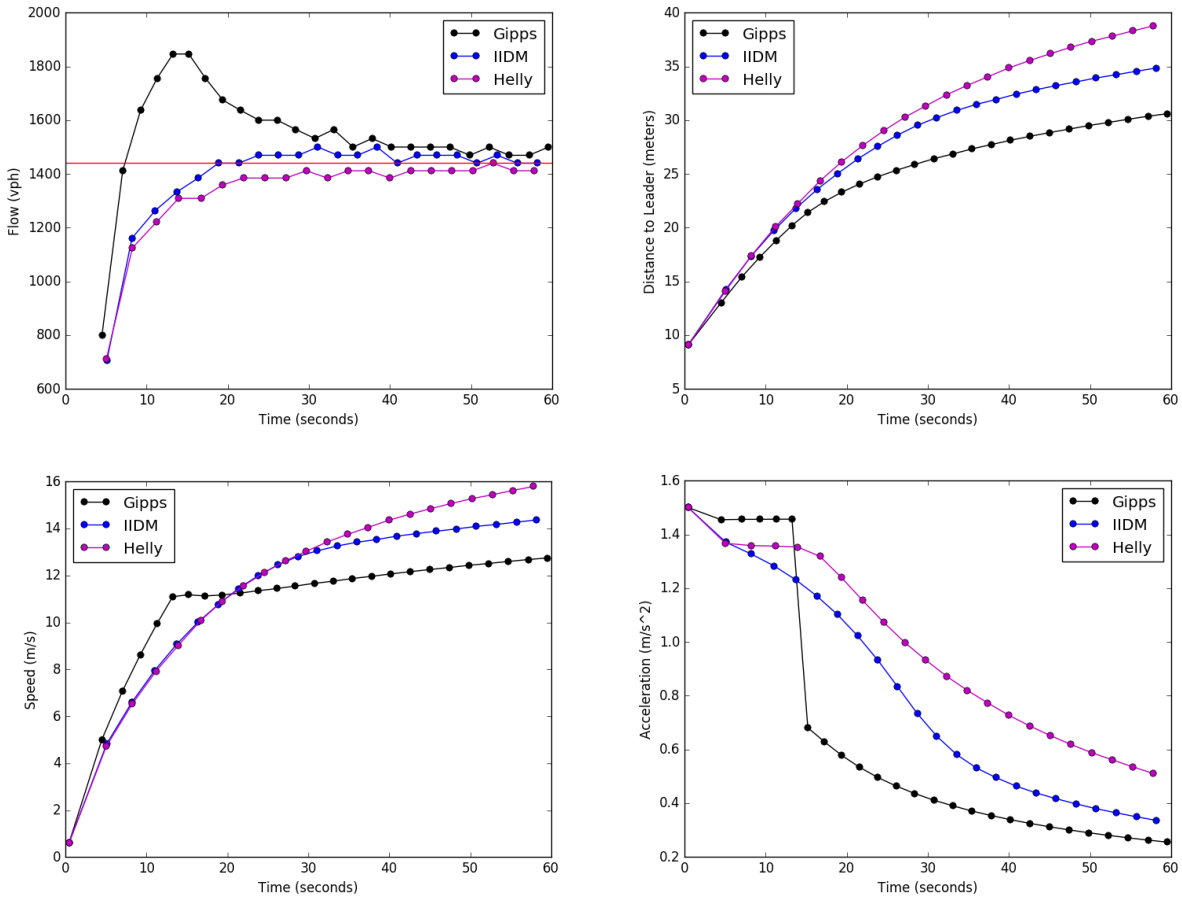

Figure 2.15: Experiment with a free road ahead: comparison of point measurements of flow, distance to leader, speed and acceleration at the detector location between the three car following models.

in the top three trajectory plots. The first vehicle is governed by the car following model just as everyone else, but its leader is infinitely far. From the acceleration and speed plots one can see that in the Gipps and the Helly models the first vehicle accelerates with maximal acceleration $a_{\max}$ until reaching the maximal speed, at which point the acceleration instantaneously drops to 0. In the IIDM, the first vehicle accelerates with $a^*(t)$ from equation (2.3.5), approaching the maximal speed asymptotically.

The most important for the intersection throughput assessment, however, is the traffic behavior at the stop bar — at the detector location indicated in Figure 2.13. Figure 2.15 presents the point measurments obtained from this detector location, with each dot corresponding to a vehicle passing the detector. Flow (top left) is computed for a vehicle passing the detector based on the time passed after the previously detected vehicle, taken as a headway $\theta(t)$, which is then inverted ($f(t) = 1/\theta(t)$) and converted to vehicles per hour (vph). The red horizontal line corresponds to the equilibrium flow, in our case — 1440 vph, when vehicles

move at maximal speed. Gap (top right) between vehicles as well as speed (bottom left) are monotonically increasing, while acceleration (bottom right) is monotonically decreasing.

As is evident from plots in Figure 2.15, Gipps model produces rather aggressive car following pattern to the point that it manages to push through the intersection 26 vehicles per minute, two more than would pass through the intersecton in an equilibrium flow (24 vehicles per minute), while IIDM and Helly model push through 23 and 22 vehicles per minute respectively — see the middle row (free road ahead) of Table 2.3. What is interesting about this observation, is that with the Gipps model one could argue that a signal would increase the road throughput by creating pulses in the vehicle flow, as the one in Figure 2.15 (top left). Moreover, the smaller the signal cycle, the bigger will be the throughput increase. This is counterintuitive and, likely, unrealistic. IIDM and Helly model can be tuned to behave more agressively by increasing their parameters δ_1, δ_2 in IIDM and α_1, α_2 in Helly. Neither of these two models, however, can reach the throughput result of Gipps.

Experiment with a red light downstream.

Let us modify the experiment setup by introducing the second intersection downstream of the first one, where vehicles have to stop at the red light — Figure 2.16 depicts the modified configuration.

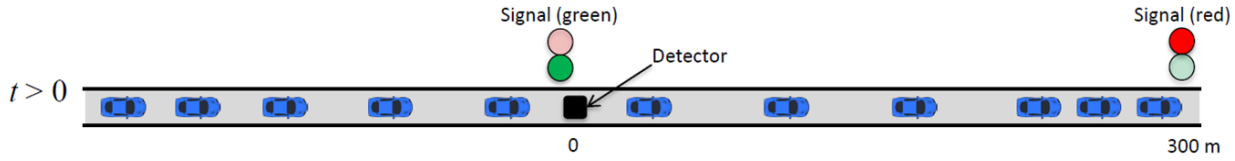

Figure 2.16: Signal turns green at time $t = 0$, and vehicles start moving. The first vehicle encounters red light in the next intersection 300 meters downstream.

In this experiment, the second intersection is 300 meters away from the first one. This distance is enough to hold 33 vehicles in the queue (see Table 2.1 for default values of the car length l and the minimal gap $g_{\min}$), which is more than the most aggressive, Gipps, car following model can send in one minute.

It is important to note that if instead of any car following model we were using a Point Queue model with limited or unlimited queues, such as in [27], we would be able to send as many vehicles through the first intersection, as our saturation flow setting would allow. In the case of our example, if we set the saturation flow to 24 vehicles per minute (equal to our equilibrium flow), after 1 minute of green light in

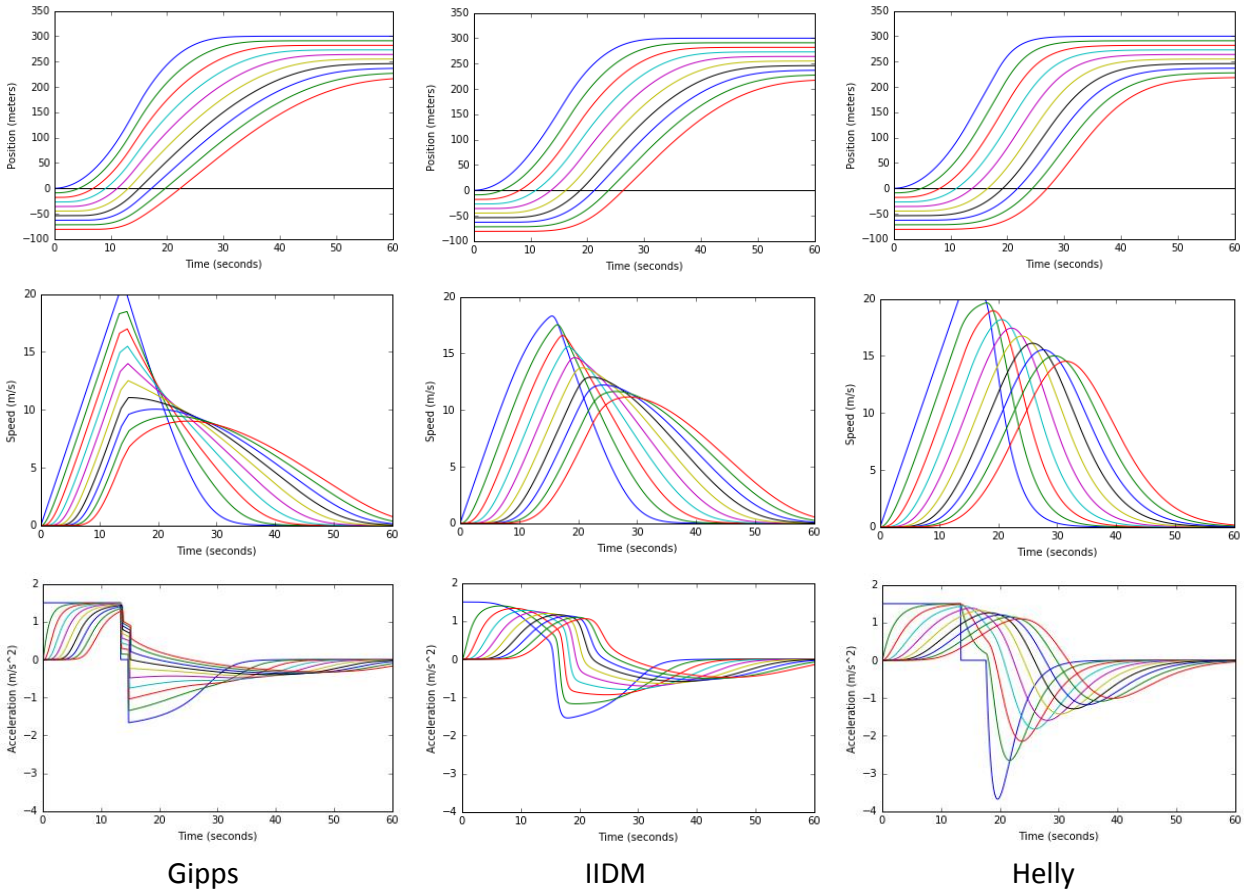

Figure 2.17: Experiment with a red light ahead: comparison of vehicle trajectories, speeds and accelerations between the three car following models.

the first intersection, 24 vehicles would be transferred from the first queue to the next, in front of the second intersection. The car following model, on the other hand, exhibits the braking effect that propagates back and reduces the vehicle flow though the first intersection. In the experiment with the red light downstream we study the impact of this braking effect on the throughput of the first intersection.

Figure 2.17 shows trajectories, speeds and accelerations of the first ten vehicles from the queue computed by the three car following models. The first signal is at position 0 indicated by the horizontal black line in the top three trajectory plots, and the second signal is at position $x_s = 300$. To make the first vehicle stop at x_s, we place a "blocking vehicle" in front at position

$$x_b = x_s + g_{\min} + l = 300 + 4 + 5 = 309,$$

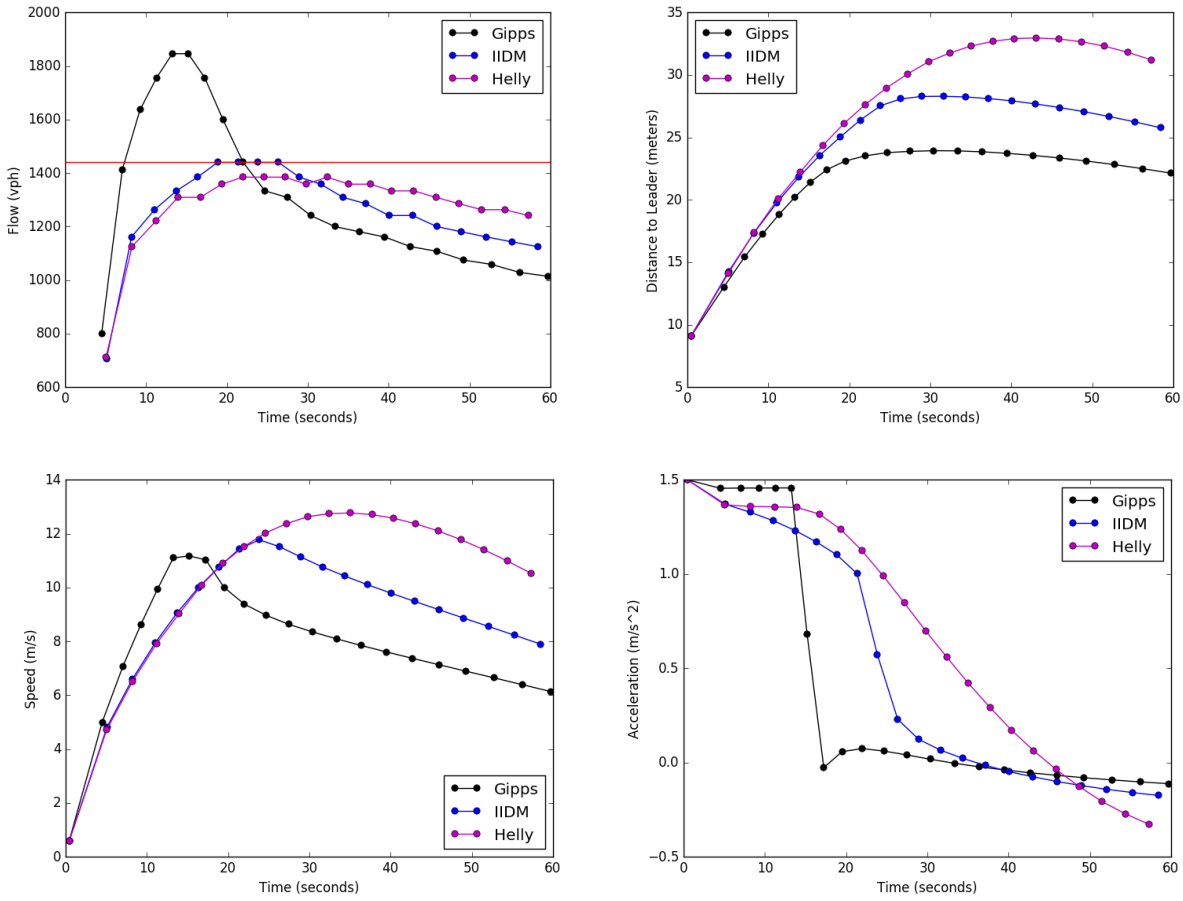

Figure 2.18: Experiment with a red light ahead: comparison of point measurements of flow, distance to leader, speed and acceleration at the detector location between the three car following models.

with velocity $v_b = 0$. Governed by the car following model, the first vehicle stops at position x_s to maintain the minimal gap with this virtual "blocking vehicle". In our case, the first vehicle in the Gipps and the Helly models reaches the maximal speed before starting to brake. Moreover, in the Helly model the first vehicle continues with the maximal longer than in Gipps, allowing the second vehicle to almost reach the maximal speed, which then leads to prohibitively sharp deceleration jump. In contrast, in IIDM the first vehicle starts to brake earlier than in Gipps and Helly models, even before reaching the maximal speed, resulting in smooth speed curves.

Point measurements taken at the detector location, shown in Figure 2.16, and presented in Figure 2.18, indicate the reduction in flow through the first intersection as the result of the braking propagation. Gipps, IIDM and Helly models manage to send 22, 21 and 21 vehicles per minute respectively through the first intersection — see the middle row (red light ahead) of Table 2.3. As before, the red horizontal line in the

top left plot corresponds to the equilibrium flow, in our case — 1440 vph, when vehicles move at maximal speed. These plots also indicate the reactiveness of the studied car following models: how fast the cars upstream react to the behavior of the first vehicle. Given the IIDM and Helly model parameter values from Table 2.2, Gipps model has the shortest reaction time, followed by IIDM and then, by Helly model.[5]

Experiment with different accelerattion levels.

Now, let us explore how throughput of the first intersection in our two previous experiments depends on the maximal acceleration $a_{\max}$. We repeat both experiments, with the free road and with the red light ahead, for three different values of $a_{\max}$: 0.8, 1.5 (our default) and 2.5 m/s^2.

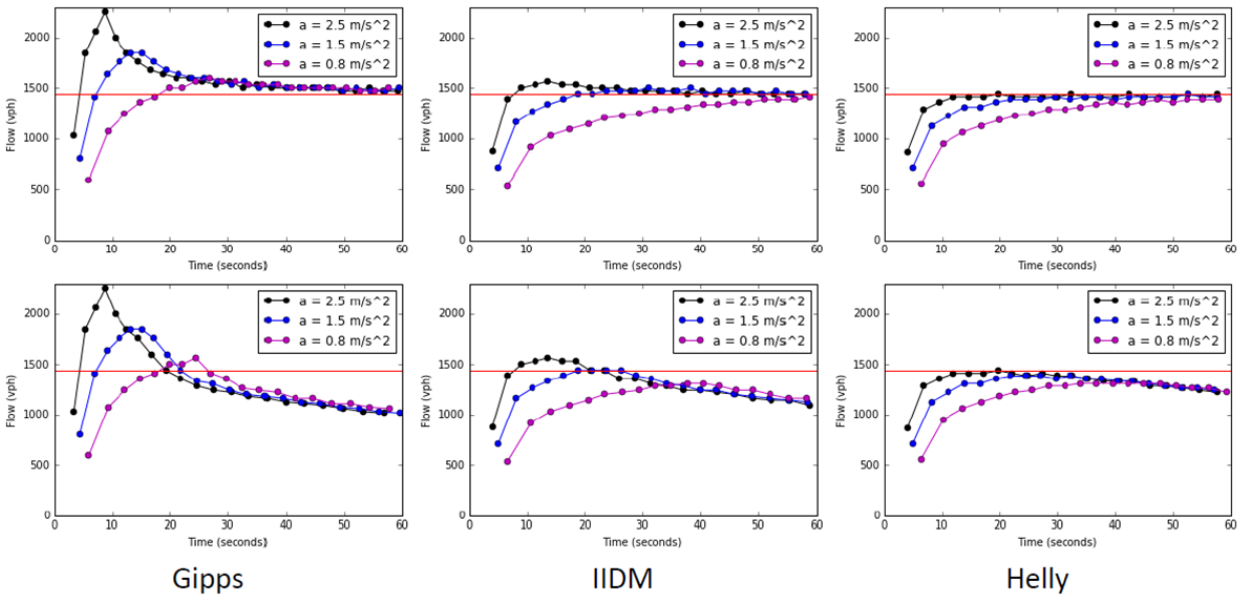

Figure 2.19: Comparing flows for different values of $a_{\max}$ for two experiments — with the free road (top), and with the red light ahead (bottom).

Value of $a_{\max}$	Type of experiment	Gipps model	IIDM	Helly model
0.8 m/s^2	free road ahead	23	20	20
	red light ahead	20	19	20
1.5 m/s^2	free road ahead	**26**	23	22
	red light ahead	22	21	21
2.5 m/s^2	free road ahead	**27**	**24**	23
	red light ahead	22	22	22

Table 2.3: Summary of three experiments — intersection throughput in vehicles per minute. Values equal to or exceeding the equilibrium flow, 24 vehicles per minute, are given in bold.

[5]Reactiveness of the two latter models can be somewhat increased by increasing parameters δ_1, δ_2 for IIDM and α_1, α_2 for Helly model.

Figure 2.19 presents the point measurements obtained from the detector location for the cases of free road (top) and red light downstream (bottom). Table 2.3 summarizes the throughput results for all the model-accelertion-experiment combinations.

The main findings of this experiment are:

- with low $a_{\max}$ and braking effect, Helly model produces larger throughput than IIDM, whereas generally the opposite is true;
- with low $a_{\max}$, IIDM and Helly model behave similarly;
- with high $a_{\max}$ and braking effect, the all three models produce the same throughput;
- braking effect reduces the impact of $a_{\max}$ parameter on throughput.

To perform a spacial analysis of the traffic flow shock wave propagation for different values of $a_{\max}$, we have to translate the car following behavior into a *macroscopic* model, which we do next.

2.3.2 Micro-to-Macro Translation

Macroscopic models describe traffic in terms of density, and speed. The road is divided into $1,\ldots,N$ links, and the state of the system at time t is given by the density-speed pair $\{\rho_i(t), V_i(t)\}_1^N$. Table 2.4 contains the notation used in macro-modeling.

Symbol	Description	Default value
Δx_i	Length of link i.	$\Delta x_i = 5$ m.
t, Δt	Time and the model time step (same as in the car following model).	$\Delta t = 0.05$ s.
$\rho_i(t)$	Vehicle density in link i.	
ρ_J	Maximal admissible (jam) density.	$\rho_J = 1/9$ veh. per meter.
$V_i(t)$	Average traffic speed link i.	
$v_{\max}$	Maximal admissible traffic speed (same as in the car following model).	$v_{\max} = 20$ m/s.
$f_i(t)$	Vehicle flow out of link i.	
$f_0(t)$	Vehicle flow entering link 1.	

Table 2.4: Macro-modeling notation.

Vehicle density $\rho_i t)$ is computed from the gap between vehicles and the vehicle length:

$$\rho_i(t) = \frac{1}{g_i(t)+l}, \tag{2.3.9}$$

where notation $g_i(t)$ defines average gap between vehicles that are in link i at time t. Obviously, $\rho_i(t) \leq \rho_J = \frac{1}{g_{\min}+l}$.

Every time step, density values in each link are updated according to the conservation law:

$$\rho(t+\Delta t) = \rho_i(t) + \frac{\Delta t}{\Delta x_i}\left(f_{i-1}(t) - f_i(t)\right), \quad i = 1,\ldots,N, \tag{2.3.10}$$

where $f_i(t) = \rho_i(t)V_i(t)$, and the entering flow $f_0(t)$ is given.

The speed equation is derived from vehicle speed. For points (t,x) on the trajectory of a vehicle, we can write:

$$v(t) = V(t,x).$$

The change in position during one time step Δt can be expressed by the first order Taylor expansion around (t,x):

$$\begin{aligned} v(t+\Delta t) &= V(t+\Delta t, x+v(t)\Delta t) \\ &= V(t,x) + \frac{\partial V(t,x)}{\partial t}\Delta t + \frac{\partial V(t,x)}{\partial x}v(t)\Delta t \\ &= V(t,x) + \left(\frac{\partial V}{\partial t} + V(t,x)\frac{\partial V}{\partial x}\right)\Delta t. \end{aligned}$$

At the same time, from the car following model we have:

$$v(t+\Delta t) = v(t) + a(t)\Delta t.$$

Thus, we get:

$$V(t,x)+\left(\frac{\partial V}{\partial t}+V(t,x)\frac{\partial V}{\partial x}\right)\Delta t = V(t,x)+a(t)\Delta t,$$

which, after cancelling $V(t,x)$ and dividing both sides of the equation by Δt, yields:

$$\frac{\partial V}{\partial t}+V(t,x)\frac{\partial V}{\partial x} = a(t).$$

Discretizing this equation in time and space, we can write:

$$\frac{V_i(t+\Delta)-V_i(t)}{\Delta t}+V_i(t)\frac{V_i(t)-V_{i-1}(t)}{\Delta x_i} = a_i(t), \quad i=1,\ldots,N,$$

and $V_0(t)=V_1(t)$.

Thus, we obtain the speed equation:

$$V_i(t+\Delta t) = V(t)+\left(a_i(t)-V_i(t)\frac{V_i(t)-V_{i-1}(t)}{\Delta x_i}\right)\Delta t. \tag{2.3.11}$$

Here $a_i(t)$ is defined by the car following model.

- For Gipps model, following (2.3.3), we have:

$$a_i(t) = \min\left\{a_{\max}, \frac{v_{\max}-V_i(t)}{\Delta t}, \frac{-V_i(t)-b\tau+\sqrt{(b\tau)^2+(V_{i+1}(t))^2+2b\left(\frac{1}{\rho_i(t)}-\frac{1}{\rho_J}\right)}}{\Delta t}\right\}, \tag{2.3.12}$$

  $i=1,\ldots,N$; $V_{N+1}=v_{\max}$.

- For IIDM, following (2.3.4), we have:

$$a_i(t) = \begin{cases} a_{\max}\left(1-\frac{g_{d,i}(t)}{g_i(t)}\right), & \text{if } \frac{g_{d,i}(t)}{g_i(t)}\geq 1, \\ a_i^*(t)\left(1-\left(\frac{g_{d,i}(t)}{g_i(t)}\right)^{\delta_1 a_{\max}/a_i^*(t)}\right), & \text{otherwise,} \end{cases} \tag{2.3.13}$$

where

$$a_i^*(t) = a_{\max}\left(1 - \left(\frac{V_i(t)}{v_{\max}}\right)^{\delta_2}\right), \tag{2.3.14}$$

while the actual gap, $g_i(t)$, and the desired gap, $g_{d,i}(t)$, can be expressed through density:

$$g_i(t) = \frac{1}{\rho_i(t)} - l, \quad i = 1,\ldots,N, \tag{2.3.15}$$

and

$$g_{d,i}(t) = \frac{1}{\rho_J} - l + \max\left\{0, V_i(t)\tau + \frac{V_i(t)(V_i(t) - V_{i+1}(t))}{2\sqrt{a_{\max} b}}\right\}, \ i = 1,\ldots,N; \ V_{N+1} = v_{\max}. \tag{2.3.16}$$

- For Helly model, following (2.3.7), we have:

$$a_i(t) = \min\left\{a_{\max}, \frac{v_{\max} - V_i(t)}{\Delta t}, \alpha_1\left(V_{i+1}(t) - V_i(t)\right) + \alpha_2\left(\frac{1}{\rho_i(t)} - \frac{1}{\rho_J} - V_i(t)\tau\right)\right\}, \tag{2.3.17}$$

$i = 1,\ldots,N$; $V_{N+1} = v_{\max}$.

As an example, we reproduced the experiment with the red light ahead and the red light at the second intersection in the macroscopic environment. The road is split into 240 links, each with length $l = 5$ meters. The first signal is located at link 50. The initial condition is:

$$\rho_i(0) = \rho_J = \frac{1}{g_{\min} + l} = \frac{1}{4+5} = 1/9, \quad 1 = 1,\ldots,49;$$
$$\rho_i(0) = 0, \quad i = 50,\ldots,N = 240;$$
$$V_i(0) = 0, \quad i = 1,\ldots,N = 240.$$

The second signal with the red light is in link 110 (300 meters downstream of the first one), which translates into condition:

$$f_{110}(\cdot) = 0.$$

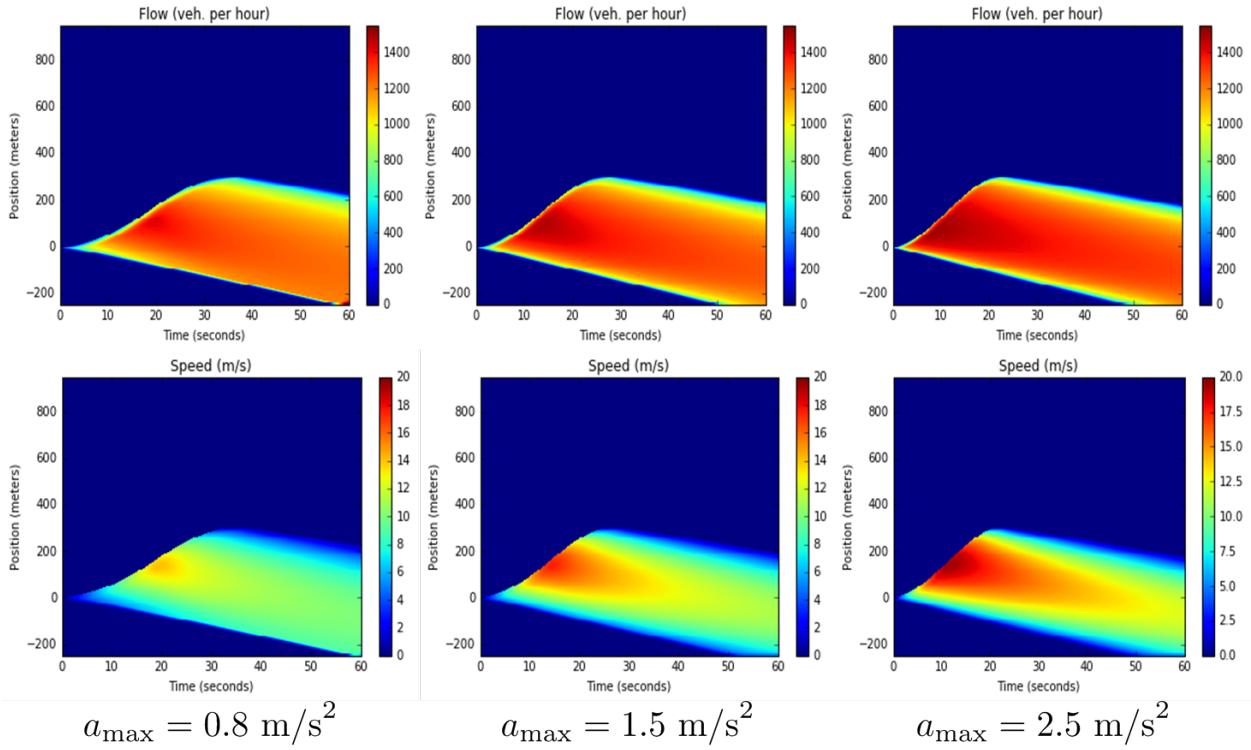

Figure 2.20: Flow (top) and speed (bottom) contours generated by the IIDM-induced macroscopic model in the experiment with the red light downstream for $a_{\max} = 0.8$, 1.5 and 2.5 m/s^2.

Figure 2.20 presents the flow and speed contours, produced by the simulation of 60 seconds of the IIDM-induced macroscopic model for $a_{\max} = 0.8, 1.5$ and 2.5 m/s^2. Here, the horizontal axis represents time in seconds and the vertical axis — space in meters, where cars travel from bottom to top. The locations of the first and the second signals are at positions 0 and 300 on the vertical axis respectively.

2.3.3 Effect off Adaptive Cruise Control (ACC) and Cooperative Adaptive Cruise Control (CACC)

We will now explore the impact of ACC and CACC vehicles on intersection throughput. To do that, we repeat two experiments described in Section 2.3.1 — the case of free road and the case of red light downstream — but this time, throwing ACC and CACC vehicles into the traffic mix. Values of car following parameters for ordinary, ACC- and CACC-enabled vehicles are given in Table 2.5. As we can see, ACC and CACC vehicles can maintain shorter distances to the car in front.

We assume that the ACC vehicle has the same car following model as the ordinary one, just with different

Vehicle type	Reaction time τ (seconds)	Minimal gap $g_{\min}$ (meters)
Ordinary	2.05	4
ACC-enabled	1.1	3
CACC-enabled	0.8	3

Table 2.5: Values of reaction time τ and minimal gap $g_{\min}$ for ordinary, ACC- and CACC-enabled vehicles.

τ and $g_{\min}$. CACC vehicle behaves just as ACC, with ACC τ and $g_{\min}$, if it follows an ordinary vehicle, but if it has another CACC car in front, it assumes different car following behavior, which we call *CACC car following model*.

Denote $a_{IIDM}(t)$ the acceleration function defined by (2.3.4). Define *constant-acceleration heuristic (CAH)* acceleration function [46] (Chapter 11):

$$a_{CAH}(t) = \begin{cases} \frac{v^2(t)\bar{a}_l(t)}{v_l^2(t)-2(x_l(t)-x(t)-l)\bar{a}_l(t)}, & \text{if } v_l(t)(v(t)-v_l(t)) \le -2(x_l(t)-x(t)-l)\bar{a}_l(t), \\ \bar{a}_l(t) - \frac{(v(t)-v_l(t))^2\Theta(v(t)-v_l(t))}{2(x_l(t)-x(t)-l)} & \text{otherwise,} \end{cases} \tag{2.3.18}$$

where

$$\bar{a}_l(t) = \min\left\{\dot{v}_l(t), a_{\max}\right\},$$

and

$$\Theta(z) = \begin{cases} 1, & \text{if } z \ge 0, \\ 0, & \text{otherwise.} \end{cases}$$

Now we specify the CACC car following model [46] (Chapter 11):

$$a_{CACC}(t) = \begin{cases} a_{IIDM}(t), & \text{if } a_{CAH}(t) \le a_{IIDM}(t), \\ a_{CAH}(t) + b\tanh\left(\frac{a_{IIDM}(t)-a_{CAH}(t)}{b}\right), & \text{otherwise.} \end{cases} \tag{2.3.19}$$

As before, we run the free road and the red light downstream experiments using Gipps, IIDM and Helly car following models. For each of these models, we compute the intersection throughput, when portion of ACC (CACC) vehicles in the initial queue. Thus, we evaluate 72 cases, each defined by: (1) experiment — free road or red light downstream; (2) car following model — Gipps, IIDM, Helly; (3) ACC or CACC; and (4)

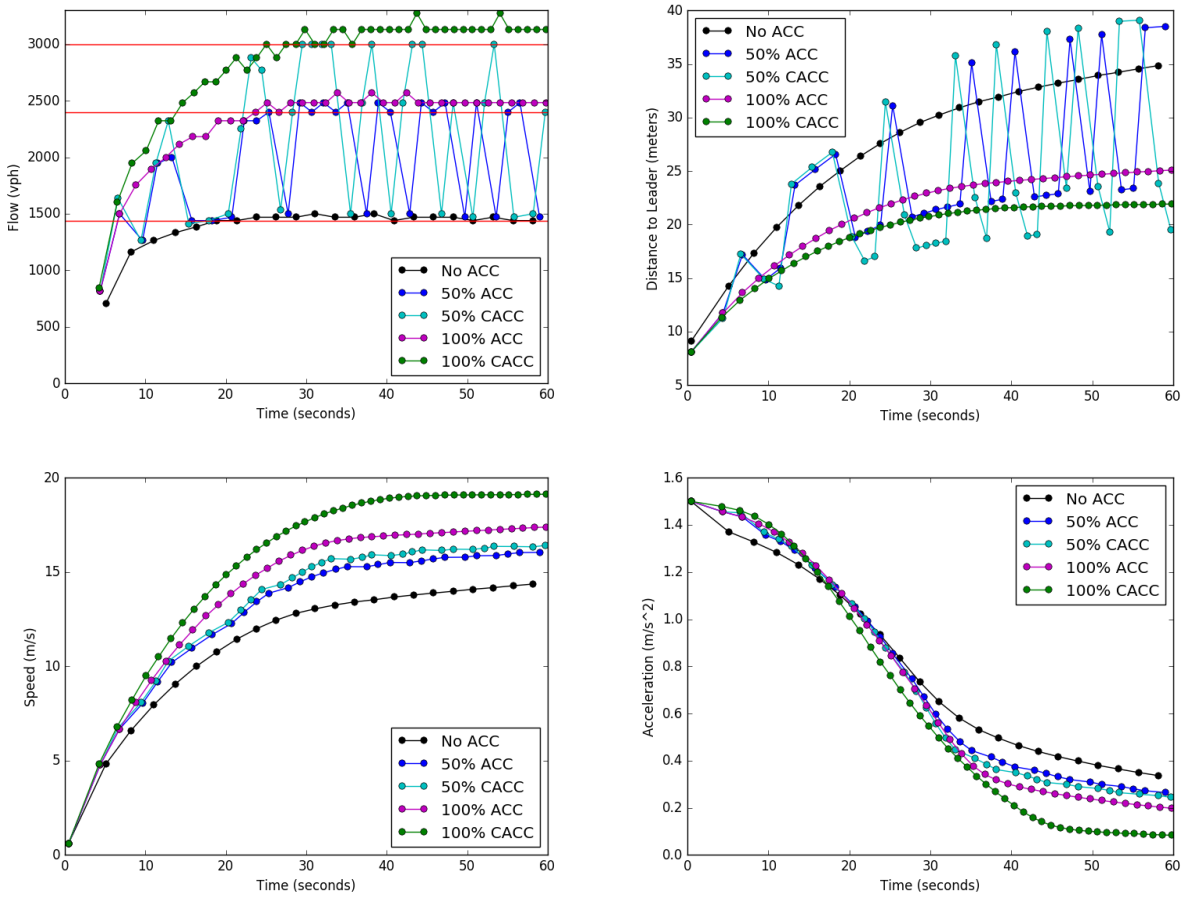

Figure 2.21: Single intersection case: comparison of point measurements of flow, distance to leader, speed and acceleration at the detector location for different portions of ACC/CACC traffic.

percentage of ACC (CACC) — 10, 25, 50, 75, 90 and 100%.

Figures 2.21 and 2.22 compare flows, gaps, speeds and acceleration obtained at the detector location (see Figures 2.13 and 2.16) for 0, 50 and 100% ACC (CACC) penetration rate. Three horizontal red lines on flow plots in both figures correspond to equilibrium flows with 0% ACC (CACC), with 100% ACC and with 100% CACC penetration rate. These flows are computed as $3600/\theta_e$, where θ_e is given by (2.3.8) with τ and $g_{\min}$ from Table 2.5, yilding 1440, 2400 and 3000 vehicles per hour respectively. In the flow and distance to leader plots, one can see how 50% ACC curves jump between the no ACC and 100% ACC curves — for ordinary vehicles it is similar to the no ACC curve, and for an ACC vehicle it is similar to 100% ACC curve. 50% CACC curves in the same plots jump between three curves — no ACC, 100% ACC and 10% CACC. This is because a CACC vehicle following an ordinary one behaves like ACC vehicle.

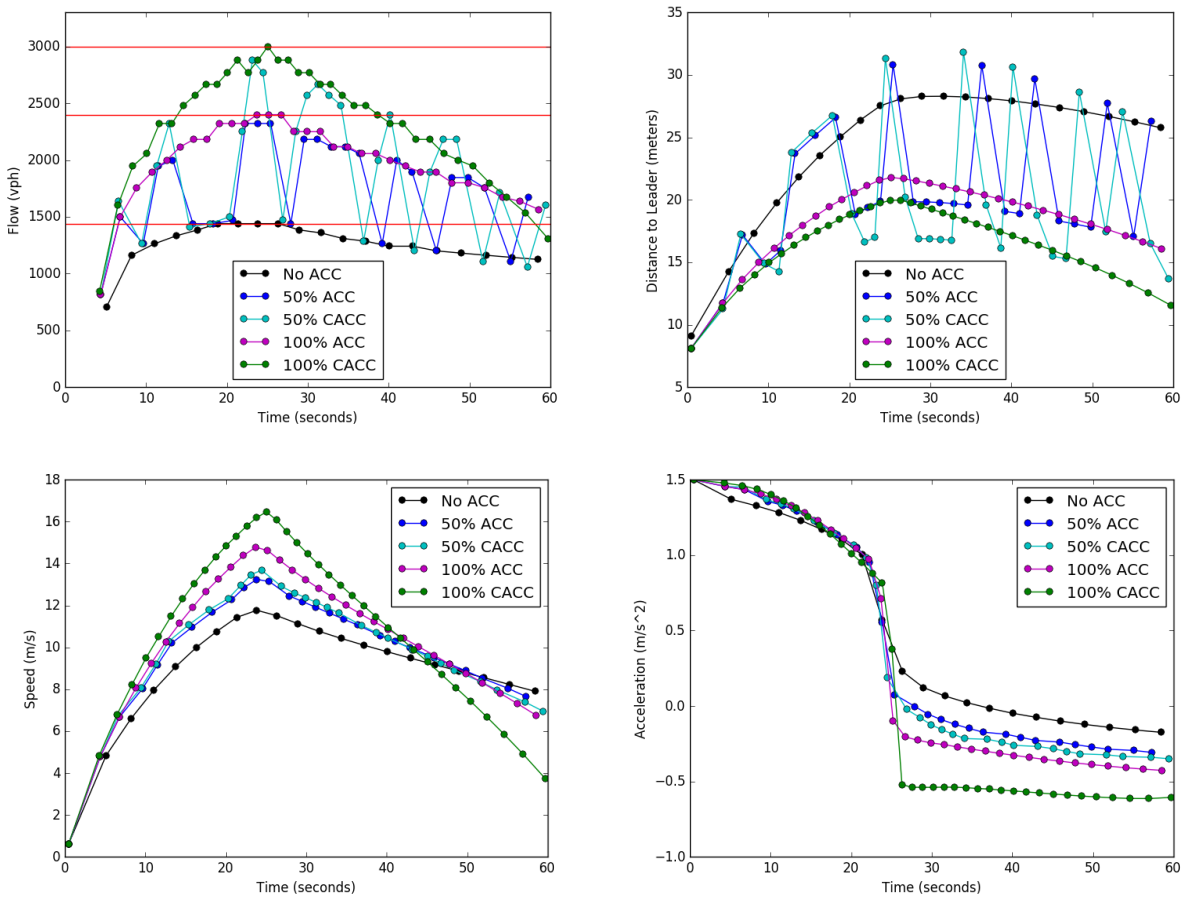

Figure 2.22: Case with red light downstream: comparison of point measurements of flow, distance to leader, speed and acceleration at the detector location for different portions of ACC/CACC traffic.

For a given ACC (CACC) penetration rate less than 100%, the intersection throughput is sensitive to the distribution of ACC (CACC) vehicles in the initial queue. For example, if 25% all vehicles in the initial queue are ACC-enabled, and all of them are concentrated at the head of the queue, we would get higher vehicle count at the detector location after one minute, than we would with 50% ACC penetration rate when all ACC-enabled vehicles are concentrated at the tail of the queue. In another example, 50% CACC penetration rate would not produce any gain over 50% ACC penetration rate, if ordinary and ACC/CACC vehicles interleave — one ordinary, one ACC/CACC, one ordinary, and so on — since CACC provides benefit over ACC in terms of throughput only when some CACC vehicles have other CACC vehicles directly in front.

To mitigate this ACC (CACC) distribution bias, for each of the cases with ACC (CACC) penetration rate less than 100%, we run 100 one-minute simulations of the three car following models and record vehicle counts

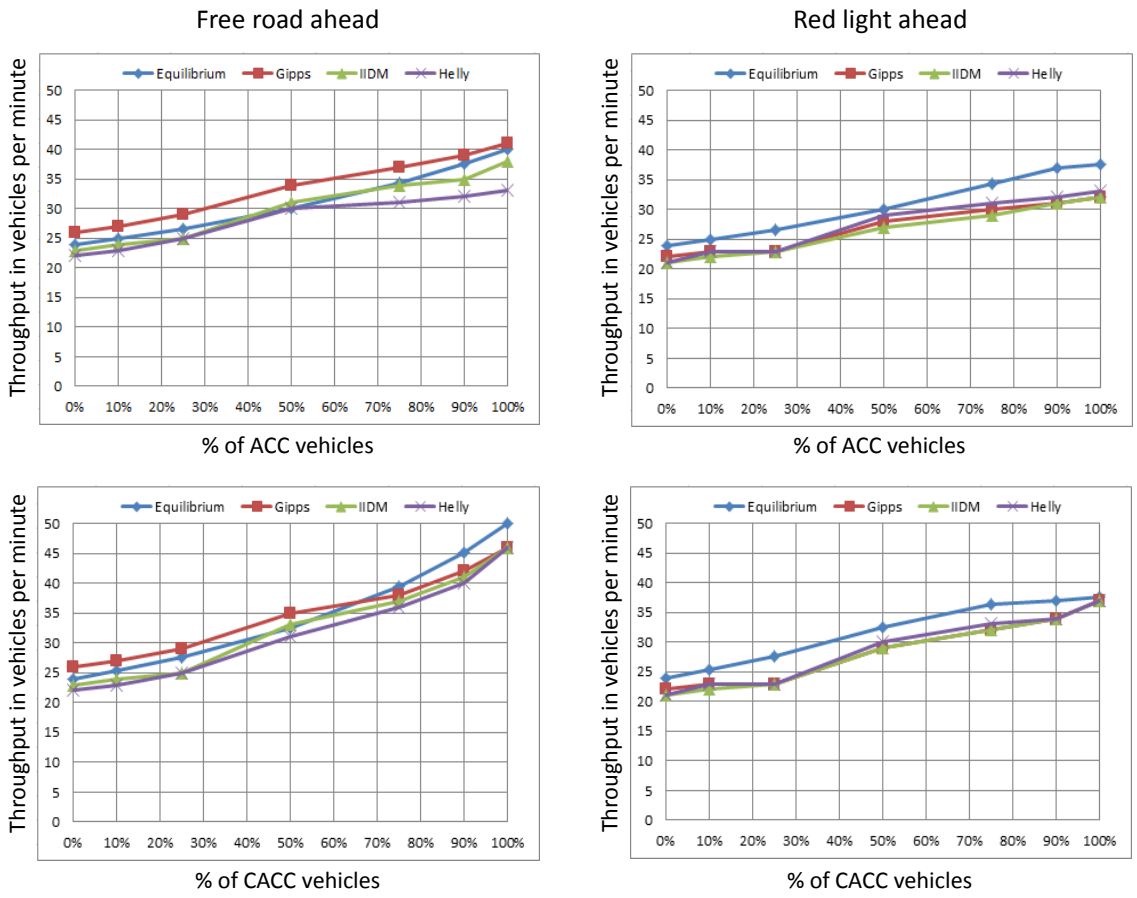

Figure 2.23: Intersection throughput as a function ACC/CACC portion of traffic computed with Gipps, IIDM and Helly car following models for two cases — free road downstream (left) and red light downstream (right).

at the detector location, then take the median vehicle count. For 100% penetration rate the ACC (CACC) distribution is trivial, and hence, a single simulation for each case is enough. The intersection throughput results for all the 72 cases, together with throughput values from Table 2.3 obtained for 0 ACC (CACC) penetration rate, are presented at the four plots in Figure 2.23.

Note that in each of the four plots in Figure 2.23, in addition to the three curves corresponding to car following models, there is a curve corresponding to the *equilibrium* traffic flow. These equilibrium curves are computed as follows. Denote $\lambda \in [0,1]$ a portion of ACC (CACC) vehicles in the initial queue; $\tau^{[C]ACC}$ and $g_{\min}^{[C]ACC}$ the reaction time and minimal gap for ACC (CACC) vehicles, whose values are given in Table 2.5.

The average headway in the equilibrium state is obtained by modifying expression (2.3.8):

$$\theta(\lambda) = \lambda\tau^{[C]ACC} + (1-\lambda)\tau + \frac{\lambda g_{\min}^{[C]ACC} + (1-\lambda)g_{\min} + l}{v_{\max}}. \tag{2.3.20}$$

Then, the equilibrium flow in vehicles per minute is given by:

$$f(\lambda) = 60/\theta(\lambda). \tag{2.3.21}$$

This formula is sufficient for the case when there is a free road ahead. In the case of the red light downstream, however, we are restricted by the capacity of the link connecting the two intersections. To account for that, we modify (2.3.21) accordingly:

$$f(\lambda) = \min\left\{\frac{60}{\theta(\lambda)}, \frac{k\Delta}{\lambda g_{\min}^{[C]ACC} + (1-\lambda)g_{\min} + l}\right\}, \tag{2.3.22}$$

where Δ is the length of the link between the two intersections, and k is the number of lanes in that link. In our experiment, $\Delta = 300$, and $k = 1$.

2.3.4 Platoon Model

Vehicles equipped with CACC technology can communicate with one another to form platoons. These platoons can increase the throughput of intersections by decreasing headways between successive vehicles. In simulation, platoon management and formation is divided into three phases:

1. identifying vehicles that can be grouped into platoons;
2. Adjusting parameters of leaders and followers in platoons; and
3. performing maintenance on the platoon.

This hierarchy is modeled by the state machine in Figure 2.24.

To form a platoon, vehicles must be in sequence with one another on a given lane. However, vehicles need not share the same final destination and are free to switch lanes or leave the platoon if necessary. If an

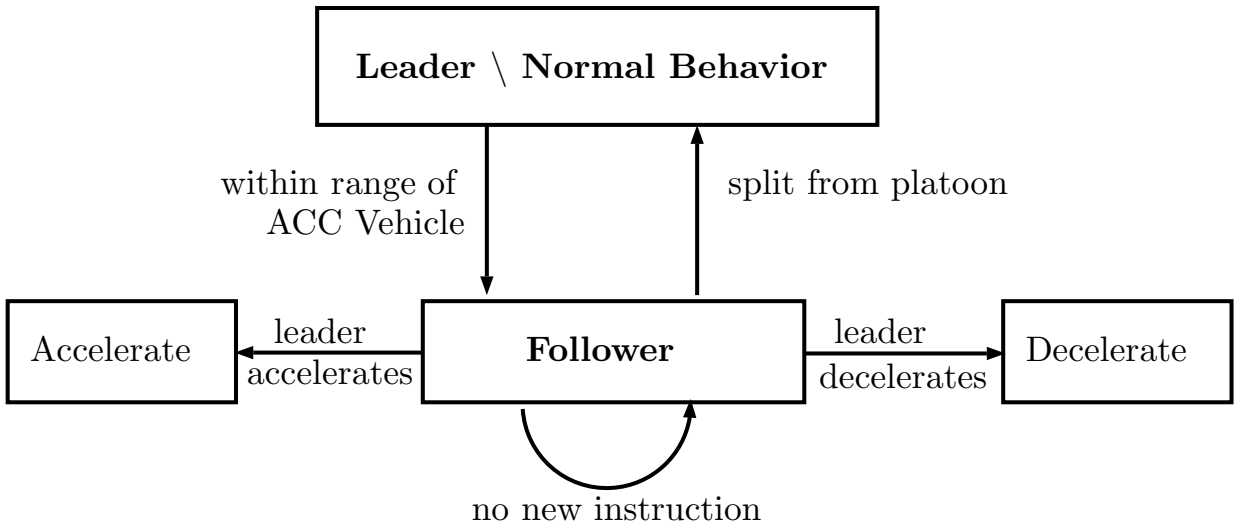

Figure 2.24: State machine describing platoon behavior.

intermediate vehicle in the platoon changes its route by making a turn or changing lanes, the platoon splits into two: one platoon for the vehicles ahead of the intermediate vehicle and another for all the vehicles behind.

A platoon's lead vehicle has the same properties as ACC vehicles. An isolated CACC vehicle is a leader of a platoon of size 1. When a platoon leader comes into range of another CACC vehicle in front, it joins the platoon becoming a follower. Followers have reduced headway and travel much closer to one another than standalone vehicles. In addition, followers are able to receive information from the leader, such as to accelerate after a green light at an intersection or to decelerate approaching an obstacle, e.g. red light downstream.

Since followers are not bound to the same route as the platoon leader, they are free to separate. After leaving the platoon, the headway and acceleration parameters are restored to their original values. This can happen for example when the follower changes its route or becomes separated from the rest of platoon, e.g., due to switching traffic signal as it crosses the intersection.

Figure 2.25 displays a screenshot of SUMO simulation run in graphical mode. It shows how vehicles cross intersection at Montrose Road and Tildenwood Drive (AP3321 with respect to Figure 2.1). Ordinary vehicles are colored in blue. [C]ACC vehicles with no followers (standalone) are colored in green. Platoon leaders are colored in cyan, and followers are white.

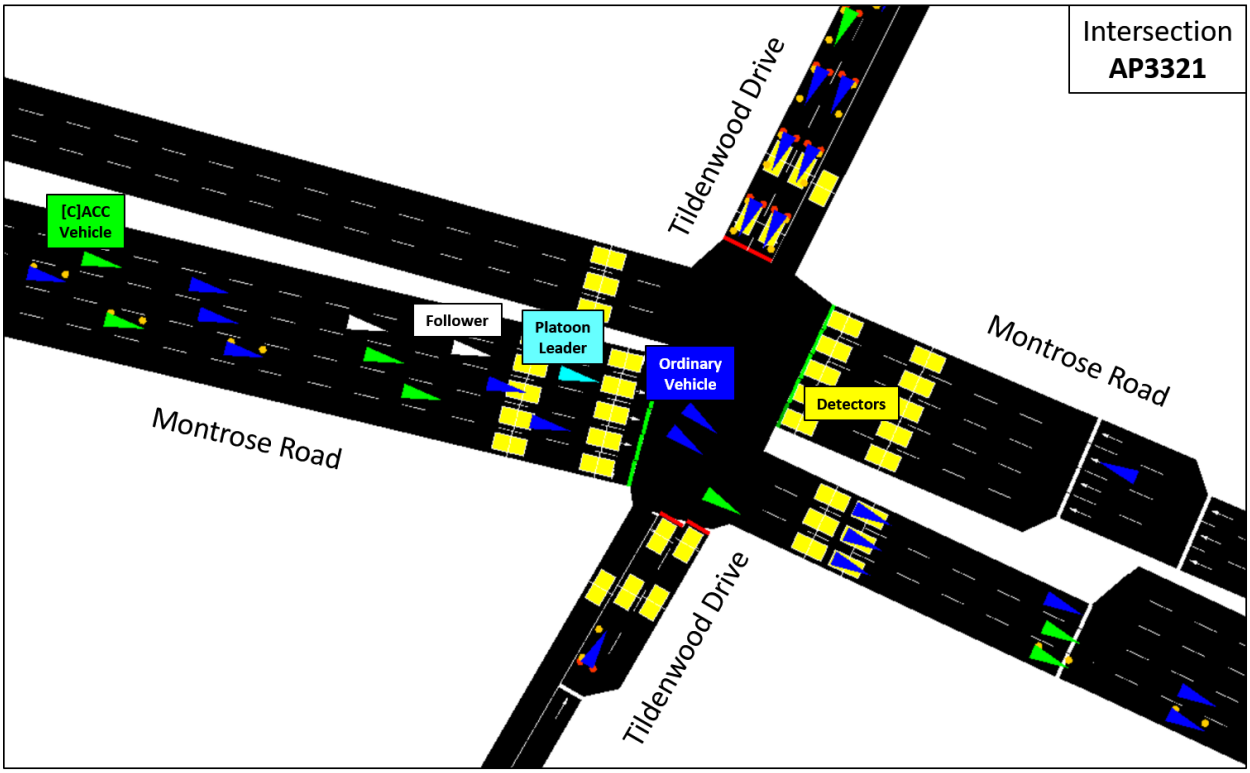

Figure 2.25: SUMO screenshot — ordinary, standalone [C]ACC vehicles and platoons are crossing intersection AP3321 (Montrose Road and Tildenwood Drive). Platoon leader and follower, as well as standalone [C]ACC and ordinary vehicles are labeled accordingly.

Next, we discuss SUMO simulation results.

2.4 Simulation of Rollins Park Network

To study the impact of platooning, we built the SUMO [25] simulation model of the Rollins Park network (Figure 2.1) with seven major intersections, shown in Figure 2.26. IIDM and CACC car following models were implemented in C++ within SUMO, and platoon management, presented as a state machine in Figure 2.24, was implemented in Python using SUMO/TraCI API [2]. The corresponding source code repository can be accessed at [1].

Using vehicle counts and estimated turn ratios, we generated 1 hour of origin-destination (O-D) travel demand data with a route assigned to each vehicle. These travel demand data together with signal plans constitute input for the simulation model — see Figure 2.2.

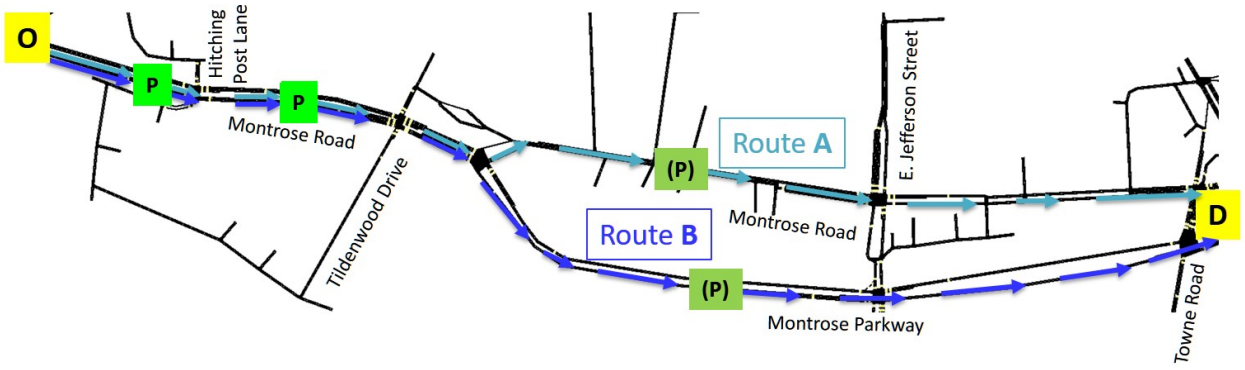

Figure 2.26: Rollins Park network — O-D pair with routes A and B. Labels 'P' indicate links, where platoons form, when platooning is enabled. Labels '(P)' indicate additional links with optional platooning, when it is enabled.

We focused our study on the single O-D pair with two routes, A and B, connecting origin (O) and destination (D) — see Figure 2.26. Routes A and B coincide in the beginning, following Montrose Road, and split at intersection AP3300 into Montrose Road (route A) and Montrose Parkway (route B).

General approach to congestion analysis on an arterial network is as follows. Intersections, where under a given demand a vehicle queue on at least one approach keeps growing are identified as bottlenecks. If rearranging the duration of green phases within a cycle leads to a periodic queue behavior — when a queue grows then dissolves — on all intersection approaches, then this intersection bottleneck is due to poor control. If, on the other hand, with any phase split we continue observing at least one increasing queue, then we have a situation of excessive demand.

Figures 2.27-2.28 show queue dynamics at the routes A and B approach to the intersection of Montrose Road and Hitching Post Lane (AP3323). Vehicle queue measured in SUMO does not grow beyond the storage capacity of a road link, where this queue is measured. Once the link storage capacity is reached, queue spills back into the upstream link. In Figures 2.27-2.28, queue size reaches the storage capacity of 36. Actually, it grows further, but SUMO reports only the maximum halted vehicles in this particular link. What we observe from the queue dynamnics plot, though, is that after a certain time peiod, this vehicle queue is never fully served. In other words, number of vehicles in the queue does not go to zero. It means, that green phase for the vehicles on routes A and B at intersection AP3323 is too short for the given demand. It so happens that increasing green phase for the movement corresponding to routes A and B is not a viable option, because that would create a backup on the cross street, Hitching Post Lane. Thus, we have a case

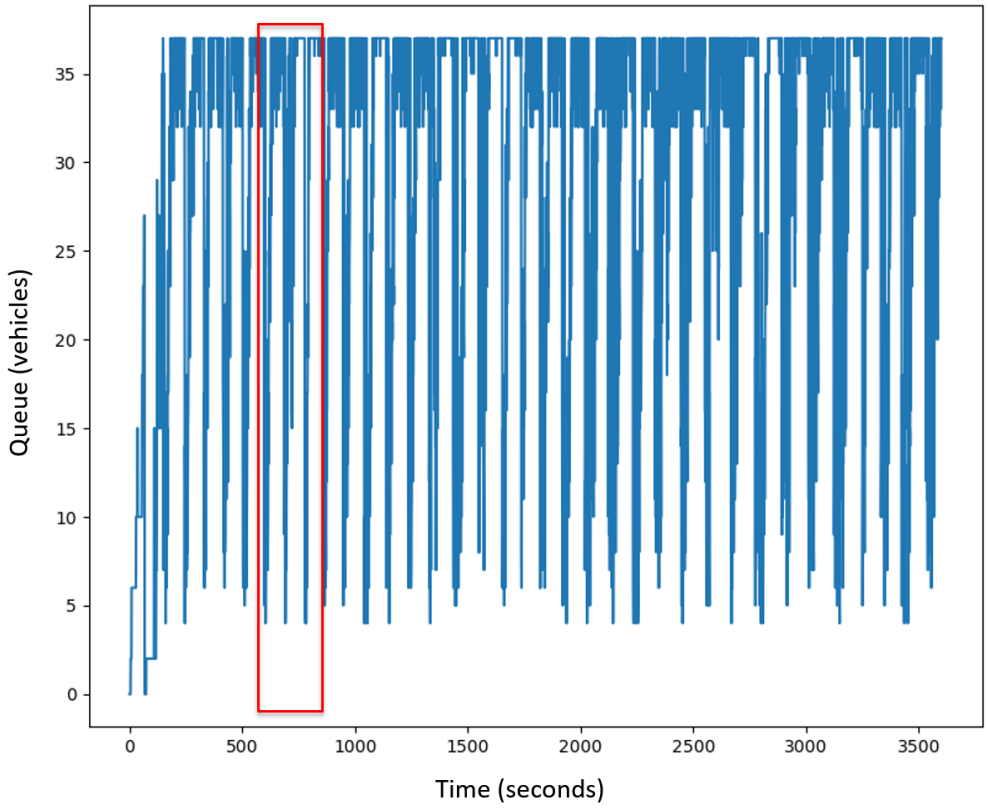

Figure 2.27: Queue dynamics at the route A (B) approach to the intersection of Montrose Road and Hitching Post Lane (AP3323).

of excessive demand at intersection AP3323. The problem of excessive demand may be mitigated with decreasing vehicle headways — through platoon creation.

We enabled platooning on two links labeled 'P' in Figure 2.26 — upstream and downstream links of intersection AP3323 on routes A and B. Then, we ran a series of simulation scenarios varying the fraction of ACC (CACC) vehicles from 0 to 75%. In each simulation two vehicle classes were modeled: ordinary vehicles and ACC (or CACC) vehicles. In simulations with CACC vehicles platoons were formed in those two links, where platoning was enabled. The same number of vehicles was processed in each simulation. The rates and locations at which cars were generated were identical in all scenarios to eliminate the variance in randomly generated routes. For cases of 0, 25, 50 and 75 percent ACC (CACC) penetration rate, we computed average travel time for routes A and B. Table 2.6 lists the resulting mean travel times.

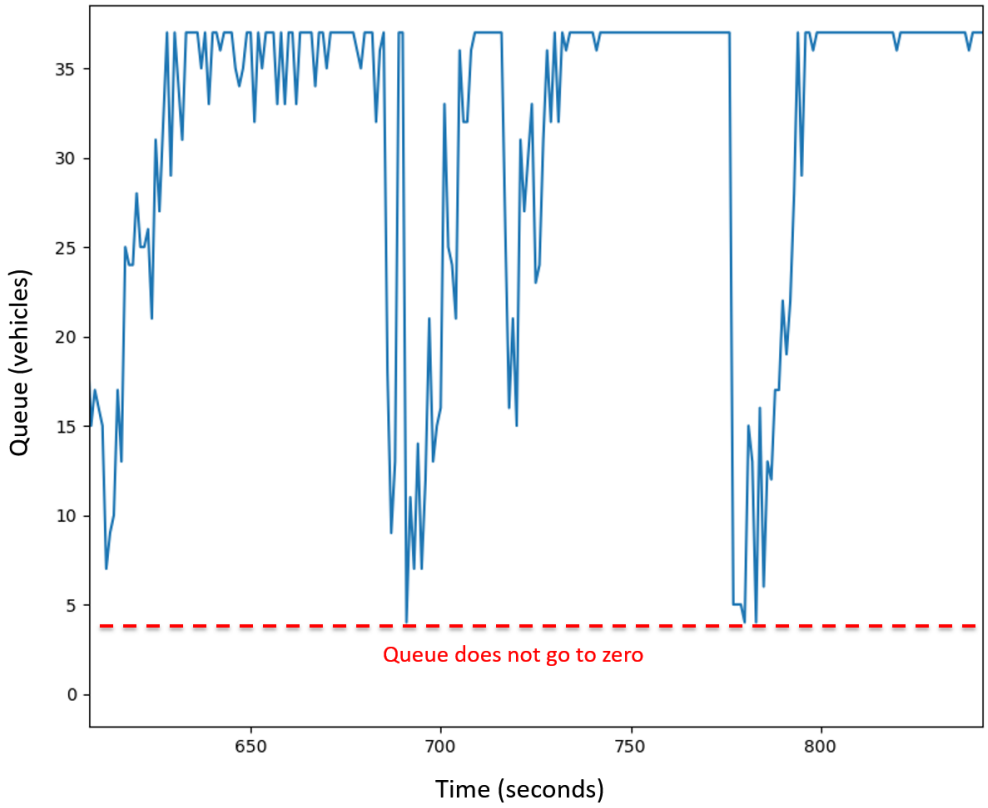

Figure 2.28: Zoomed-in queue dynamics from Figure 2.27 — queue does not empty.

We can see that ACC vehicles alone (without platooning) reduce the travel time along both routes A and B. Travel time improvement achieved by CACC over ACC should be attributed to the higher throughput of intersection AP3323, resulting in smaller queues and thus, smaller waiting times in queues, formed upstream of this intersection. Note that ordinary vehicles show reduced travel times, although [C]ACC vehicles have larger gains. Another observation is that the biggest travel time improvement happens when CACC penetration rate goes from 25 to 50%. The reason is that with 25% CACC penetration rate, chances that CACC vehicles will be positioned in sequence, so that a platoon can be formed, are relatively low. So, CACC case does not show much improvement over ACC with 25% penetration rate. On the other hand, when CACC peneration rate is high at 75%, platoons become much more frequent and of larger sizes. This leads to oversaturation of the downstream link, creating a new bottleneck that offsets some of the upstream travel time gains achieved by the platooning.

[C]ACC %	Vehicle Class	Route A		Route B	
		ACC	CACC	ACC	CACC
0	ordinary	711	711	622	622
25%	ordinary	696	696	608	607
	[C]ACC	691	688	604	598
	all	695	694	607	605
50%	ordinary	671	670	553	547
	[C]ACC	665	646	539	523
	all	671	658	546	535
75%	ordinary	661	646	526	516
	[C]ACC	660	642	526	509
	all	660	643	526	511

Table 2.6: Mean travel time in seconds for varying percentage of [C]ACC vehicles on routes A and B (see Figure 2.26).

CACC %	Vehicle Class	Route A		Route B	
		Original	Additional Platooning	Original	Additional Platooning
25%	ordinary	696	695	607	607
	CACC	688	686	598	599
	all	694	693	605	605
50%	ordinary	670	672	547	548
	CACC	646	644	523	520
	all	658	658	535	534
75%	ordinary	646	646	516	515
	CACC	642	641	509	506
	all	643	642	511	508

Table 2.7: Comparing mean travel time on routes A and B from the original platooning experiment with the mean travel time, where platooning is allowed in the additional links, as indicated in Figure 2.26. Travel time is in seconds.

To see how platooning can further reduce trave times on routes A and B, we enabled it on links approaching intersections AP3319 (on route A) and AP3299 (on route B). Those additional platooning links are labeled '(P)' in Figure 2.26. Then, we re-ran simulation scenarios with 25, 50 and 75% [C]ACC portion of traffic. Average travel times for routes A and B are summarized in Table 2.7, comparing them with the results of the original experiment.

As we can see, additional platooning practically does not reduce travel time. This happens because intersections AP3319 and AP3299 are not bottlenecks, Pushing vehicles through these intersection in platoons does not qualitatively change queue dynamics at AP3319 and AP3299 on routes A and B: the green phase was sufficient to handle unplatooned traffic.

Moreover, platooning may cause a problem on cross streets. In the case of 50% CACC penetration rate, platooning pushes too much traffic through intersection AP3319 along route A blocking the link downstream of this intersection for the left-turning traffic from E. Jefferson Street. SUMO screenshot depicting this situation is presented in Figure 2.29.

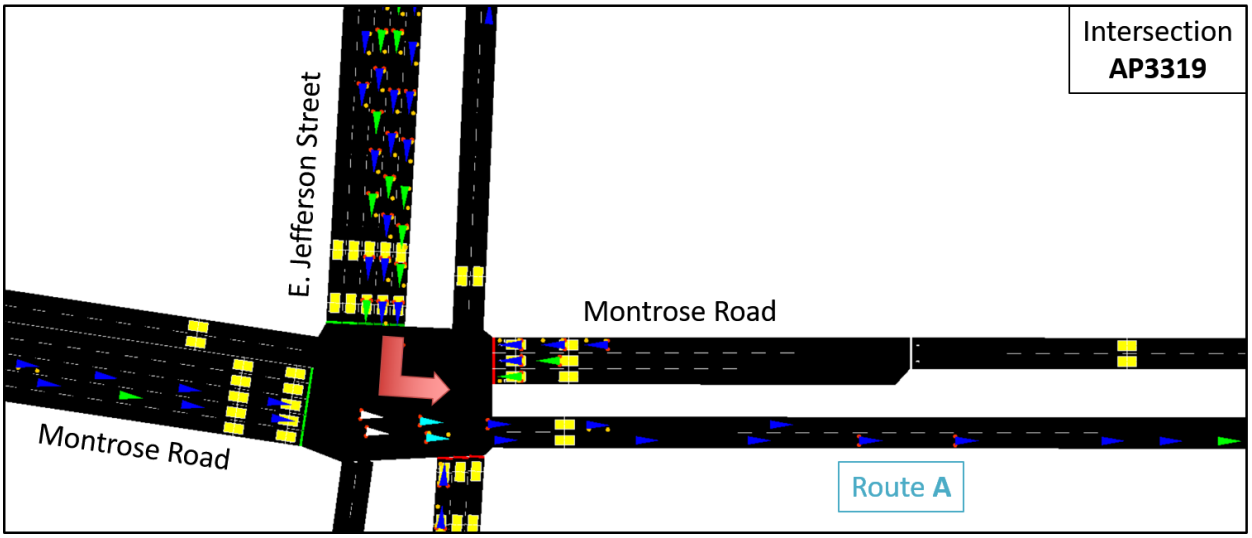

Figure 2.29: Intersection AP3319 — jam at E. Jefferson Street left turn pocket.

Thus, we can succinctly formulate the platooning rule:

platooning should be enabled only at the approaches to bottleneck intersections.

Chapter 3

Conclusion

Research conducted for the current project is an important stepping stone for building a three-level information and control system for urban networks with high-density traffic, presented in Figure 1.4. In this project we focused on elements of link-level information (SPaT estimation and prediction) and vehicle-level control (ACC and CACC). In SPaT analysis we presented several novel algorithms to estimate the residual duration of a signal phase for a semi-actuated intersection. These algorithms predict the times for all future phase transitions, based on previous phase measurements and on the real time information that locates the current time within the current phase. With respect to the vehicle-level control, we analyzed sensitivity of intersection throughput to car following models and related parameters. The Improved Intelligent Driver Model (IIDM) was chosen for traffic simulation. Finally, we implemented the platoon model in SUMO and tested it in simulation of scenarios on Rollins Park network.

The results of this project enable further investigation of the following research questions:

- How to combine vehicle flow measurements with SPaT estimation and how to use predicted vehicle flows for SPat prediction.
- Accurate SPaT prediction would enable speed advisory on links approaching the intersection to minimize stops and improve progression quality. This is important for mobility, energy efficiency and safety. However, such speed harmonization may reduce throughput of upstream intersections. The

question is how to manage traffic speed at arterial links without creating bottlenecks at upstream intersections.

- The related question is about the impact of platooning in the speed harmonization effort. Specifically, how platoons should be managed when the corresponding green phase is not long enough to accommodate all vehicles in a platoon.
- How to incorporate network-level control that will balance the vehicle load on multiple routes connecting the same O-D pair after some of these routes were enhanced by the above mentioned link-level and vehicle-level control.

These questions require further investigative research in the following areas:

1. efficient measurement data analysis, and the minimum data needed for traffic system to say observable and predictable;
2. modeling for quantitative assessment of impact platooning with speed advisory and coordination of signals at multiple intersections; and
3. implementation of related infrastructure-to-vehicle (I2V) technologies.

Bibliography

[1] Sustainable Operation of Arterial Networks: Source Code Repository. `http://github.com/ucbtrans/sumo-project`.

[2] Traffic Control Interface (TraCI) for SUMO. `http://sumo.dlr.de/wiki/TraCI`.

[3] B. Asadi and A. Vahidi. Predictive cruise control: Utilizing upcoming traffic signal information for improving fuel economy and reducing trip time. *IEEE Transactions on control systems*, 19(3), 2011.

[4] Audi. Audi shows off traffic light prediction technology. Traffic Signals, January 2014.

[5] X. Ban, R. Herring, P. Hao, and A. Bayen. Delay pattern estimation for signalized intersections using sampled travel times. *Transportation Research Record: Journal of the Transportation Research Board*, (2130):109–119, 2009.

[6] M. Bando, K. Hasebe, A. Nakayama, A. Shibata, and Y. Sugiyama. Dynamical model of traffic congestion and numerical simulation. *Physical Review E*, 51:1035–1042, 1995.

[7] M. Barth, S. Mandava, K. Boriboonsomsin, and H. Xia. Dynamic eco-driving for arterial corridors. In *IEEE Forum on Integrated and Sustainable Transportation System (FISTS)*, 2011.

[8] Trasportation Research Board. *Highway Capacity Manual*. Washington DC, 2010.

[9] M. Brackstone and M. McDonald. Car-following: A historical review. *Transportation Research, Part F: Traffic Psychology*, 2(4):181–196, 1999.

[10] R. E. Chandler, R. Herman, and E. W. Montrol. Traffic dynamics: Studies in car-following. *Operations Research*, 6:165–184, 1958.

[11] National Automated Highway System Consortium. Automated highway demo 97. https://www.youtube.com/watch?v=C9G6JRUmg_A. August 1997.

[12] C.M. Day, D.M. Bullock, H. Li, S.M. Remias, A.M. Hainen, A.L. Stevens, J.R. Sturdevant, and T.M. Brennan. Performance measures for traffic signal systems: An outcome-oriented approach. Technical report, Purdue University, Lafayette, IN, 2014. doi: 10.5703/1288284315333.

[13] S.A. Fayazi, A. Vahidi, G. Mahler, and A. Winckler. Traffic signal phase and timing estimation from low-frequency transit bus data. *IEEE Transactions on Intelligent Transportation Systems*, 16(1):19–28, February 2015.

[14] Federal Highway Administration. Traffic signal timing manual. Technical Report FHWA-HOP-08-024, U.S. Department of Transportation, 2008. http://www.ops.fhwa.dot.gov/publications/fhwahop08024/fhwa_hop_08_024.pdf, accessed August 15,2009.

[15] Federal Highway Administration. Traffic Control Systems Handbook. Technical report, US Department of Transportation, 2013. http://ops.fhwa.dot.gov/publications/fhwahop06006/index.htm.

[16] H.T. Fritzsche. A model for traffic simulation. *Traffic Engineering and Control*, (5):317–321, 1994.

[17] D. C. Gazis, R. Herman, and R. W. Rothery. Nonlinear follow-the-leader models of traffic flow. *Operations Research*, 9:545–567, 1961.

[18] P. G. Gipps. A behavioral car-following model for computer simulation. *Transportation Research, Part B: Methodological*, 15(2):105–111, 1981.

[19] D. Godbole, M. A. Kourjanski, R. Sengupta, and M. Zandonadi. Breaking the highway capacity barrier: Adaptive cruise control-based concept. *Transportation Research Record*, 1679:148–157, 1999.

[20] W. Helly. Simulation of bottlenecks in single lane traffic flow. In *Proceedings of International Symposium on the Theory of Traffic Flow*, New York, NY, 1959.

[21] S. Hoogendoorn, S. Ossen, and M. Schreuder. Empirics of multianticipative car-following behavior. *Transportation Research Record*, 1965:112–120, 2006.

[22] R. Jiang, Q. Wu, and Z. Zhu. Full velocity difference model for a car-following theory. *Physical Review E*, 64(1):017101, 2001.

[23] A. Kesting, M. Treiber, and D. Helbing. Enhanced intelligent driver model to access the impact of driving strategies on traffic capacity simulations. *Philosophical Transactions of the Royal Society A*, 368:4585–4605, 2010.

[24] E. Koukoumidis, L-S Peh, and M. Martonosi. SignalGuru: Leveraging mobile phones for collaborative traffic signal schedule advisory, 2012. Mobisys'12.

[25] D. Krajzewicz. Traffic simulation with sumo-simulation of urban mobility. In *Fundamentals of Traffic Simulation*, pages 269–293. Springer, 2010. `http://www.dlr.de/ts/en/desktopdefault.aspx/tabid-9883/16931_read-41000`, accessed 04/28/2016.

[26] S Krauss. *Microscopic Modeling of Traffic Flow: Investigation of Collision Free Vehicle Dynamics*. Phd thesis, Hauptabteilung Mobilität und Systemtechnik, Cologne, 1998.

[27] J. Lioris, R. Pedarsani, F. Y. Tascikaraglu, and P. Varaiya. Platoons of connected vehicles can double throughput in urban roads. *Submitted to Transportation Research, Part C: Emerging Technologies*, 2015. `https://arxiv.org/abs/1511.00775`.

[28] V. Milanés, S.E. Shladover, J. Spring, C. Nowakowski, H. Kawazoe, and M. Nakamura. Cooperative adaptive cruise control in real traffic situations. *IEEE Transactions on Intelligent Transportation Systems*, 15(1):296–305, 2014.

[29] A. Muralidharan, S. Coogan, C. Flores, and P. Varaiya. Management of intersections with multi-modal high-resolution data. *Transportation Research, Part C*, 68:101–112, 2016.

[30] A. Muralidharan, C. Flores, and P. Varaiya. High-resolution sensing of urban traffic. In *IEEE 17th International Conference on Intelligent Transportation Systems (ITSC)*, pages 780–785, Qingdao, China, October 8-11 2014.

[31] National Operations Center of Excellence. Implementation Guide: SPAT Challenge, 2016. `https://www.transportationops.org/spatchallenge/resources/Implementation-Guide`.

[32] G. F. Newell. Nonlinear effects in dynamics of car following. *Operations Research*, 9(2):209–229, 1961.

[33] G. F. Newell. A simplified car-following theory: A lower order model. *Transportation Research, Part B: Methodological*, 36:195–205, 2002.

[34] California PATH. Investigating the potential benefits of broadcasted signal phase and timing (SPaT) data under IntelliDrive. May 2011.

[35] L. A. Pipes. An operational analysis of traffic dynamics. *Journal of Applied Physics*, 24:274–281, 1953.

[36] J. Ploeg, B.T.M. Scheepers, E. van Nunen, N. van de Wouw, and H. Nijmeijer. Design and experimental evaluation of cooperative adaptive cruise control. In *Proceedngs of. 14th ITSC IEEE Conference*.

[37] V. Protschky, S. Feit, and C. Linnhoff-Popien. Extensive traffic light prediction under real-world conditions. *80th IEEEVehicular Technology Conference (VTC Fall)*, 2014.

[38] V. Protschky, C. Ruhhammer, and S. Feit. Learning traffic light parameters with floating car data. In *Intelligent Transportation Systems (ITSC), 2015 IEEE 18th International Conference on*, pages 2438–2443. IEEE, 2015.

[39] H. Rakha and R.K. Kamalanathsharma. Eco-driving at signalized intersections using V2I communication. In *15th International IEEE Conference on Intelligent Transportation Systems*, 2011.

[40] A. Reuschel. Fahrzeugbewegungen in der kolonne. *Oesterreichisches Ingenieur-Archiv*, 4:193–215, 1950.

[41] W. J. Schakel, B. van Arem, and B. Netten. Effects of cooperative adaptive cruise control on traffic flow stability. In *Proceedings of the 13th IEEE Conference on Intelligent Transportation Systems*, Madeira Island, Portugal, September 2010.

[42] D. Schrank, B. Eisele, and T. Lomax. 2015 Urban Mobility Report Scorecard. Technical report, Texas Transportation Institute, 2015. `http://mobility.tamu.edu`.

[43] S.E. Shladover. Why automated vehicles need to be connected vehicles. `http://www.ewh.ieee.org/tc/its/VNC13/IEEE_VNC_BostonKeynote_Shladover.pdf`. 2013.

[44] D. Swaroop. *String Stability in Interconnected Systems: An Application to a Platoon of Vehicles*. Phd thesis, University of California, Berkeley, 1994.

[45] M. Treiber, A. Hennecke, and D. Helbing. Congested traffic states in empirical observations and microscopic simulations. *Physical Review E*, 62(2):1805–1824, 2000.

[46] M. Treiber and A. Kesting. *Traffic Flow Dynamics: Data, Models and Simulation*. Springer, 2013.

[47] U.S. Public Interest Research Group. New Federal Highway Figures Reveal Ninth Consecutive Year of Americans Driving Less. http://www.uspirg.org/news/usp/new-federal-highway-figures-reveal-ninth-consecutive-year-americans-driving-le

[48] USDOT. GlidePath prototype application, October 2015. https://www.its.dot.gov/factsheets/glidepath.htm.

[49] USGAO. Intelligent Transportation Systems: Vehicle-to-Infrastructure Technologies. Technical report, United States Government Accountability Office, September 2015. GAO-15-775.

[50] B. van Arem, C. J. G. van Driel, and R. Visser. The impact of cooperative adaptive cruise control on traffic flow characteristics. *IEEE Transactions on Intelligent Transportation Systems*, 7(4):429–436, 2006.

[51] J. VanderWerf, S. Shladover, M. Miller, and N. Kourjanskaia. Effects of adaptive cruise control systems on highway traffic flow capacity. *Transportation Research Record*, 1800:78–84, 2002.

[52] C Wang and S Jiang. Traffic signal phases' estimation by floating car data. In *2012 12th International Conference on ITS Telecommunications (ITST),*, pages 568–573. IEEE, 2012.

[53] M. Wang, M. Treiber, W. Daamen, S. P. Hoogendorn, and B. van Arem. Modelling supported driving as an optimal control cycle: Framework and model characteristics. *20th International Symposium on Transportation and Traffic Theory (ISTTT)*, 80(7):491–511, 2013.

[54] R. Wiedemann. *Simulation des Strassenverkehrflusses*. PhD thesis, Universtät Karlsruhe, Band 8, Karlsruhe, Deutschland, 1974.

[55] R. Wiedemann and U. Reiter. Microscopic traffic simulation: the simulation system mission, background and actual state. Final report, Project ICARUS, Brussels, 1992.

[56] H. Xia, K. Boriboonsomsin, F. Schweizer, A. Winckler, K. Zhou, W-B. Zhang, and M. Barth. Field operational testing of eco-approach technology at a fixed-time signalized intersection. In *Intelligent Transportation Systems (ITSC), 2012 15th International IEEE Conference on*, pages 188–193. IEEE, 2012.